Side Effects of Oncologic Treatment in the Chest: Manifestations at FDG PET/CT

Jordan A. Lang, MD, PhD
Sanjeev Bhalla, MD
Dhakshinamoorthy Ganeshan, MD
Gabriel J. Felder, MD
Malak Itani, MD

Abbreviations: BPF = bronchopleural fistula, FDG = fluorodeoxyglucose, GGO = ground-glass opacities, irAE = immune-related adverse event, NSIP = nonspecific interstitial pneumonia, PE = pulmonary embolism, RV = right ventricle, SLG = sarcoid-like granulomatosis, XRT = radiation therapy

RadioGraphics 2021; 41:2071–2089

https://doi.org/10.1148/rg.2021210130

Content Codes: CH NM OI

From the Mallinckrodt Institute of Radiology, Washington University School of Medicine, 510 S Kingshighway Blvd, Campus Box #8131, St Louis, MO 63110 (J.A.L., S.B., M.I.); Division of Diagnostic Imaging, The University of Texas MD Anderson Cancer Center, Houston, Tex (D.G.); and Department of Radiology, NYU Winthrop Hospital, Mineola, NY (G.J.F.). Presented as an education exhibit at the 2020 RSNA Annual Meeting. Received April 12, 2021; revision requested May 28 and received July 3; accepted July 8. For this journal-based SA-CME activity, the authors, editor, and reviewers have disclosed no relevant relationships. **Address correspondence to** J.A.L. (e-mail: *jordan.lang@wustl.edu*).

SA-CME LEARNING OBJECTIVES

After completing this journal-based SA-CME activity, participants will be able to:

- Recognize FDG PET/CT findings that are suggestive of organizing pneumonia and provide a differential diagnosis for the underlying etiologic factor.
- Describe the pathologic time course of radiation pneumonitis following completion of XRT and the corresponding FDG PET/CT findings.
- Identify characteristic FDG PET/CT findings of sarcoid-like granulomatosis.

See rsna.org/learning-center-rg.

Fluorodeoxyglucose (FDG) PET/CT is a vital imaging technique used for staging, assessing treatment response, and restaging following completion of therapy in patients who are undergoing or have completed oncologic treatment. A variety of adverse effects from chemotherapy, targeted therapy, immunotherapy, and radiation therapy are commonly encountered in oncologic patients. It is important to be aware of the manifestations of these adverse effects seen on FDG PET/CT images to avoid misinterpreting these findings as disease progression. Furthermore, early identification of these complications is important, as it may significantly affect patient management and even lead to a change in treatment strategy. The authors focus on the FDG PET/CT manifestations of a broad spectrum of oncologic therapy–related adverse effects in the thorax, as well as some treatment-related changes that may potentially mimic malignancy.

Online supplemental material is available for this article.

Introduction

Fluorodeoxyglucose (FDG) PET/CT has a well-established role in guiding therapy for various malignancies, including staging, monitoring treatment response, and restaging following completion of therapy. In patients who are undergoing or have completed oncologic treatment, a broad spectrum of treatment-related complications are routinely encountered at FDG PET/CT, secondary to a diverse array of therapies that are broadly categorized as chemotherapy, targeted therapy, immunotherapy, or radiation therapy (XRT). In this article, we summarize by treatment type the adverse effects of oncologic therapy in the chest, as well as the manifestations of these effects seen on FDG PET/CT images (Table). Treatment-related adverse effects often involve inflammatory changes, resulting in increased FDG uptake, and it is important to distinguish these findings from malignancy or, if the findings are nonspecific, provide an appropriate differential diagnosis within the context of the patient's therapeutic history.

The biochemical mechanism of FDG PET involves cellular uptake of FDG, a glucose analog, by glucose transporter membrane proteins. Following intracellular transport, FDG is phosphorylated by hexokinase, which "traps" FDG within cells, resulting in an image that reflects the sites of increased cellular glucose metabolism. Given this mechanism, the activity seen on FDG PET images is not specific to malignant cells. Normal physiologic pattern uptake shows intense activity in organs with increased glucose metabolism such as the cerebral cortex and activated brown adipose tissue, and benign pathologic uptake is commonly due to inflammation with increased uptake by activated leukocytes. Treatment-related inflammatory processes often demonstrate FDG avidity and may mimic progressive malignancy

TEACHING POINTS

- Treatment-related adverse effects often involve inflammatory changes, resulting in increased FDG uptake.
- Atypical manifestations of organizing pneumonia such as focal hypermetabolic masslike consolidation may mimic malignancy, and the degree of FDG uptake is not a reliable method of distinguishing organizing pneumonia from malignancy, given that both of these entities can result in high FDG uptake.
- The effects of XRT are unique in that they are confined to the area of the radiation port, often with abrupt linear borders of involvement that distinguish post-XRT effects from other pathologic entities. At histopathologic analysis, radiation-induced pneumonitis demonstrates a characteristic time course following completion of XRT, with corresponding FDG PET/CT findings.
- Invasive fungal pneumonia is an important differential consideration for new hypermetabolic pulmonary nodules or masses that are concerning for metastasis or malignant recurrence, especially in patients with immunosuppression, which in many cases cannot be distinguished on the basis of clinical and radiologic findings and may require biopsy for a histopathologic diagnosis.
- Characteristic FDG PET/CT features of SLG include FDG-avid pulmonary micronodules or focal round consolidation with surrounding GGO; symmetric FDG-avid lymphadenopathy, typically with mediastinal and hilar involvement; and hypermetabolic splenic lesions. Care should be taken not to mistake SLG for hyperprogression or pseudoprogression after immunotherapy.

such as sarcoid-like granulomatosis (SLG), an immune-related adverse event (irAE) associated with checkpoint inhibitor immunotherapy and seen in oncologic patients following various therapies. In addition, uptake by leukocytes can be due to infectious causes, which are commonly seen in immunosuppressed patients after intensive chemotherapy or stem cell transplant. These infectious causes include opportunistic infections such as disseminated fungal infection, which may be mistaken for progressive malignancy. Overall, consideration of prior serial imaging findings, including knowledge of the original sites of malignancy, is of utmost importance, and combined with an understanding of characteristic FDG PET/CT findings helps to distinguish adverse treatment effects from progressive malignancy.

Other adverse effects are less likely to be mistaken for malignancy on the basis of correlative CT findings, although recognizing key imaging features that are suggestive of specific complications can expedite the clinical diagnosis to guide therapeutic management or prompt further evaluation. For example, the identification of typical findings of organizing pneumonia raises suspicion for possible drug-induced pneumonitis, and an accurate diagnosis can help guide clinical decision making—for example, potentially modifying oncologic therapy and initiating treatment of pneumonitis. Recognizing the sequelae of recurrent aspiration in a patient with a history of prior XRT adjacent to the esophagus and airways can raise concern for the possibility of an airway-esophageal fistula, even if a fistula is not directly visualized, prompting appropriate further evaluation with esophagography. In this article, we showcase the anatomic and metabolic appearances of a variety of thoracic treatment–related complications and potential mimickers of malignancy seen on FDG PET/CT images by reviewing imaging findings and providing case examples with relevant differential considerations.

Pulmonary Parenchymal Complications

Drug-induced Pneumonitis

Drug-induced pneumonitis is a relatively common adverse effect, seen in about 20 of 100 patients treated with antineoplastic agents. However, the incidence is dependent on the specific agent, dose, and concurrent therapies, among other factors (1). Although with some agents, such as bleomycin, drug-induced pneumonitis is associated with a certain cumulative dose, in many cases it is idiosyncratic (2). The clinical manifestations of drug-induced pneumonitis encompass a broad spectrum of presentations, including the variable time course from acute to chronic or insidious disease, and a wide range of clinical symptoms, from no symptoms (subclinical imaging findings) to respiratory failure.

The pathogenesis of drug-induced pneumonitis includes direct cytotoxicity to pneumocytes and alveolar capillary endothelium, immune-mediated effects resulting from cytokine release or leukocyte activation or dysregulation, and oxidative injury (3). Lung injury manifests in a limited number of histopathologic patterns with corresponding characteristic CT findings. Lung injury patterns include organizing pneumonia, nonspecific interstitial pneumonia (NSIP), eosinophilic pneumonia, diffuse alveolar damage or acute lung injury, diffuse pulmonary hemorrhage, a hypersensitivity pneumonitis–like pattern, and usual interstitial pneumonia (4,5).

Our focus is on two common lung injury patterns, organizing pneumonia and NSIP, with examples of FDG PET/CT cases provided, as a comprehensive review of lung injury patterns is beyond the scope of this article. Pathologically, organizing pneumonia demonstrates plugs of granulation tissue within distal airways and alveoli. Clinically, organizing pneumonia typically manifests with constitutional symptoms and shortness of breath, although it may be asymptomatic. Characteristic CT features include peripheral or peribronchovascular consolidation

Oncologic Treatment Side Effects Manifesting in the Chest

Side Effect Type	Chemotherapy	Immunotherapy and Targeted Therapy	Radiation Therapy
Pulmonary, airway, pleural	Pneumonitis, pulmonary edema or pleural effusion, pulmonary hemorrhage	Pneumonitis, pulmonary edema or pleural effusion, pulmonary hemorrhage, pneumothorax	Pneumonitis, pleural effusion, BPF, bronchial stenosis
Cardiovascular	Cardiomyopathy, pericarditis or myocarditis, vasculitis, venous thromboembolic disease, accelerated atherosclerosis	Cardiomyopathy, pericarditis or myocarditis, vasculitis, venous thromboembolic disease	Cardiomyopathy, valvular disease, pericarditis or myocarditis, vasculitis, accelerated atherosclerosis
Additional mediastinal	Esophagitis, rebound thymic hyperplasia	Esophagitis	Esophagitis or ulceration, esophageal fistula or stricture
Systemic	Immunosuppression	SLG	…
Chest wall	Gynecomastia (hepatotoxicity)	Osteitis or osteonecrosis, gynecomastia	Osteitis or osteonecrosis, myositis, skin thickening or fat necrosis
Malignancy	Myelodysplastic syndrome or leukemia	…	Sarcoma, breast and lung cancers, myelodysplastic syndrome or leukemia

Note.—BPF = bronchopleural fistula, SLG = sarcoid-like granulomatosis.

and/or ground-glass opacities (GGO) (Figs 1, 2). The reverse halo sign (or atoll sign) of central GGO with peripheral consolidation is specific, although it is seen in only 20% of cases (Fig 2C, 2D) (6). Bandlike and perilobular or polygonal consolidation also is a highly suggestive finding (Figs 1A, 2A, 2B) (7). Less commonly, atypical manifestations are identified and include focal or masslike consolidation, multiple nodular opacities, and diffuse centrilobular nodules (8,9).

On FDG PET/CT images, organizing pneumonia demonstrates increased FDG uptake, with the greatest uptake in areas of consolidation and the degree of uptake corresponding directly to disease activity (10). Atypical manifestations of organizing pneumonia such as focal hypermetabolic masslike consolidation may mimic malignancy, and the degree of FDG uptake is not a reliable method of distinguishing organizing pneumonia from malignancy, given that both of these entities can result in high FDG uptake (9). In such cases, biopsy may be required to distinguish these atypical manifestations from recurrent malignancy (Fig 3). In addition, hypermetabolic mediastinal lymph nodes are commonly seen; they were reported in 76% of organizing pneumonia cases in one study involving 50 patients (9). Multiple studies have investigated the potential of dual–time-point FDG PET/CT in differentiating malignancy from inflammatory processes. This examination involves an additional delayed acquisition with expected increased FDG uptake by malignancies at the delayed time point and relatively decreased FDG uptake by inflammatory processes due to presumed faster washout of FDG from benign tissue. However, the results have been mixed (11). The 2013 European Association of Nuclear Medicine and Society of Nuclear Medicine and Molecular Imaging guidelines for the use of FDG PET/CT in the setting of infection and inflammation do not support a clinical role of dual–time-point imaging in differentiating infection from cancer (12).

Toxic agents resulting in organizing pneumonia include bleomycin, cyclophosphamide, methotrexate, immune checkpoint inhibitors, mammalian target of rapamycin inhibitors, anaplastic lymphoma kinase inhibitors, and epidermal growth factor receptor inhibitors, among others (4,5). Although organizing pneumonia is a well-known oncologic therapy–related complication, it may be caused by a variety of etiologic factors; hence, correlation with the clinical history is key. In addition to medication-related conditions, the differential diagnosis for organizing pneumonia includes viral pneumonia, graft versus host disease, connective tissue disease and autoimmune disorders, and electronic cigarette– and vaping-associated lung injury (8,13). When idiopathic, organizing pneumonia is frequently known as cryptogenic organizing pneumonia.

NSIP is a lung injury pattern that typically has a more insidious onset of progressive respiratory symptoms, often with a restrictive pattern of lung disease at pulmonary function testing (14).

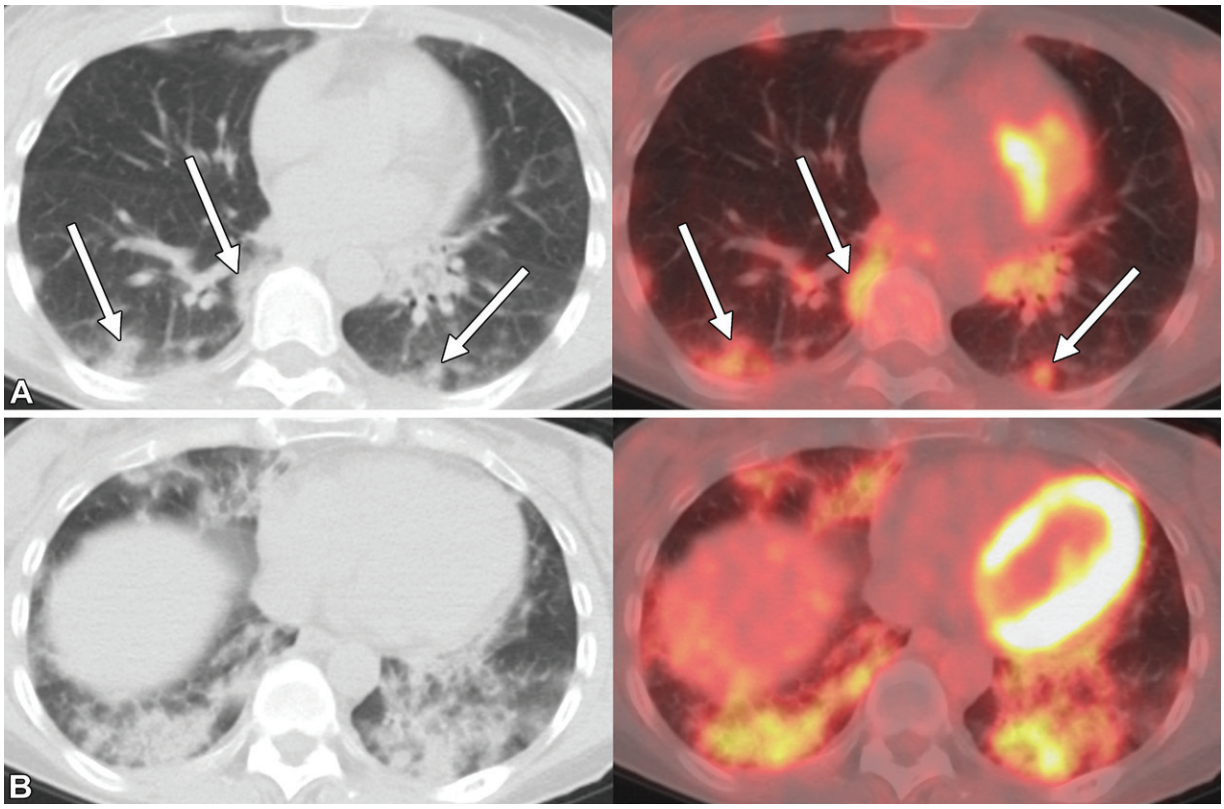

Figure 1. Checkpoint inhibitor immunotherapy–induced organizing pneumonia in a 58-year-old woman with metastatic melanoma, which was treated with nivolumab. Transaxial CT (left) and fused FDG PET/CT (right) images obtained at the level of the mid **(A)** and lower **(B)** thorax to monitor treatment response show new hypermetabolic peripheral and peribronchovascular consolidation and GGO, which are more confluent at the lung bases. This distribution, with findings of peripheral bandlike and small round consolidations in the mid lungs (arrows in **A**), is indicative of organizing pneumonia pattern pneumonitis. Nivolumab was discontinued, and follow-up surveillance FDG PET/CT (not shown) after 9 months of discontinuation showed improved consolidation and GGO, with uptake similar to that in the blood pool. After 2 years, the findings had essentially resolved.

There are two types of NSIP, a cellular type and a fibrotic type, with the latter being more common. Histopathologic analysis reveals interstitial thickening with chronic inflammatory changes with or without fibrosis, and absence of the typical features of other interstitial lung diseases (14). Characteristic CT features include basilar predominant peripheral GGO that may demonstrate subpleural sparing, which may be helpful when present (15). In addition, the fibrotic type shows reticulation with thickening of bronchovascular bundles and traction bronchiectasis without honeycombing (Fig 4) (15).

On FDG PET/CT images, NSIP demonstrates increased FDG uptake associated with inflammatory lesions (GGO and consolidation) and fibrotic lesions (reticulation) (16). The areas of FDG uptake have been proposed to represent active and potentially reversible disease. One study (17) has shown that visual assessment of the extent of FDG uptake in NSIP might be useful for the prediction of pulmonary function improvement with immunosuppressive treatment. Hypermetabolic mediastinal lymph nodes also are commonly seen with NSIP (16). Toxic agents resulting in NSIP include methotrexate, carmustine, immune checkpoint inhibitors, mammalian target of rapamycin inhibitors, and epidermal growth factor receptor inhibitors, among others (4,5). In addition to drug-induced NSIP, the differential diagnosis includes NSIP from connective tissue disease or autoimmune disorders, HIV infection, and graft versus host disease (14,15).

Radiation-induced Pneumonitis

The effects of XRT are unique in that they are confined to the area of the radiation port, often with abrupt linear borders of involvement that distinguish post-XRT effects from other pathologic entities. At histopathologic analysis, radiation-induced pneumonitis demonstrates a characteristic time course following completion of XRT, with corresponding FDG PET/CT findings (Fig 5A) (18).

Radiation-induced acute pneumonitis begins as an exudative phase characterized by a pattern of diffuse alveolar damage lung injury within the irradiated field. There is a lag in the clinical and imaging manifestations, which typically appear after 4 weeks following XRT completion

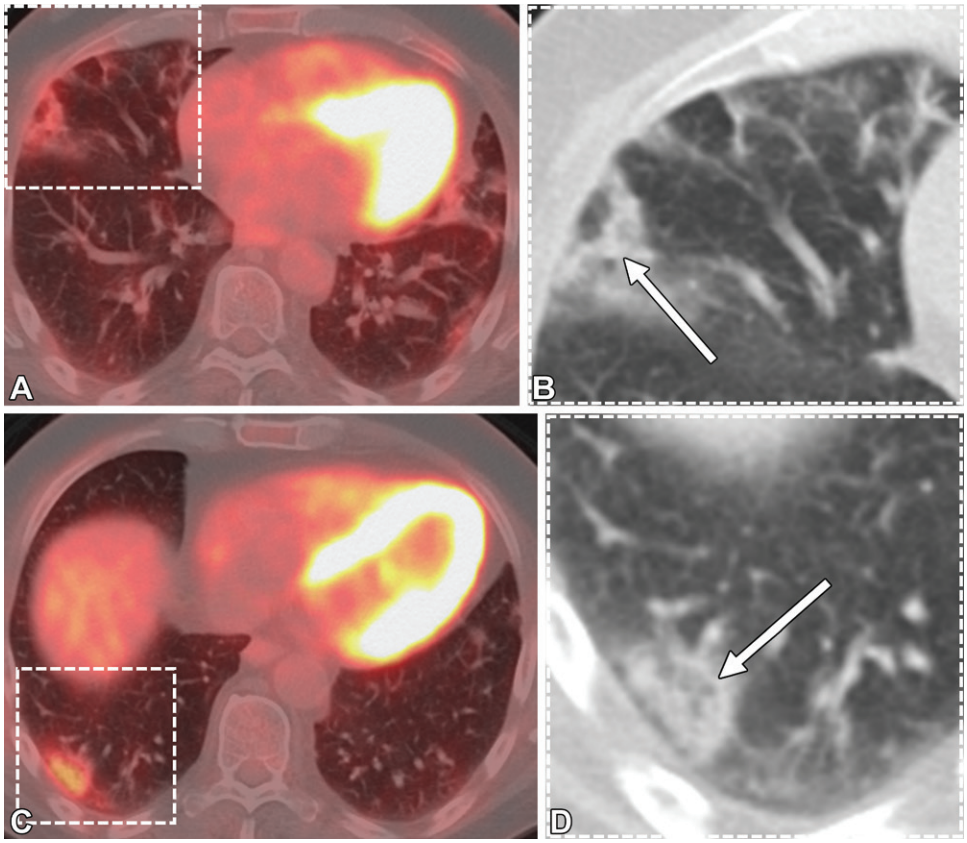

Figure 2. Organizing pneumonia secondary to graft versus host disease in a 60-year-old man with mantle cell lymphoma after allogenic stem cell transplant. **(A, C)** Transaxial fused restaging FDG PET/CT images 2 years after stem cell transplant show new, mildly hypermetabolic peripheral consolidation and GGO, with the inset area in **A** magnified in the corresponding CT image **(B)** and the inset area in **C** magnified in the corresponding CT image **(D). (B, D)** The magnified CT images highlight characteristic CT findings of organizing pneumonia, including a perilobular pattern of consolidation (arrow in **B**) and the reverse halo sign (or atoll sign) of consolidation with central GGO (arrow in **D**).

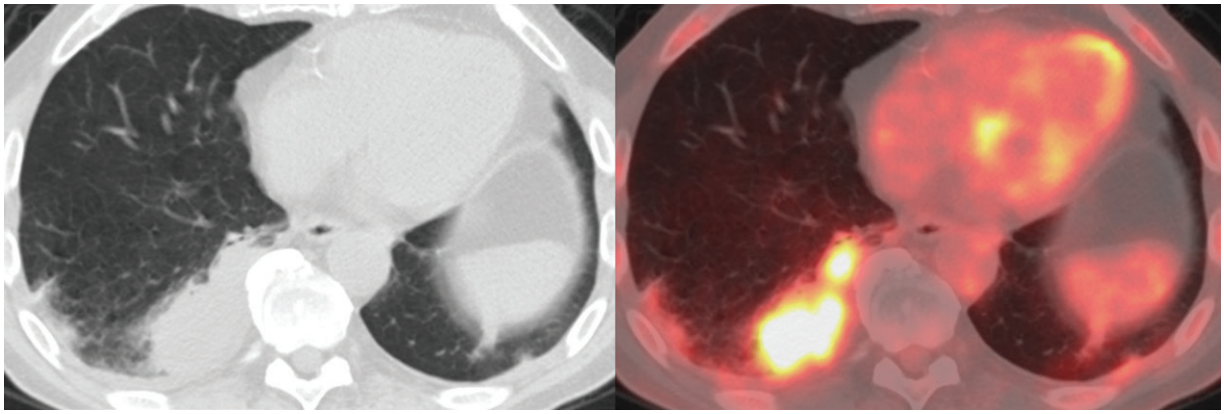

Figure 3. Atypical manifestation of organizing pneumonia in a 68-year-old man with previously treated bilateral non–small cell lung cancer who was recently started on targeted kinase inhibitor ibrutinib therapy for chronic lymphocytic leukemia. Transaxial CT (left) and fused FDG PET/CT (right) images for monitoring treatment response 3 months after initiation of ibrutinib therapy demonstrate a new markedly hypermetabolic masslike consolidation in the right lower lobe. There was also hypermetabolic right paratracheal, right hilar, and subcarinal lymphadenopathy (not shown). Given the concern for recurrent lung cancer, biopsies of the masslike consolidation and lymph nodes were performed, and histopathologic analysis revealed organizing pneumonia for the masslike consolidation and chronic lymphocytic leukemia for the right paratracheal, right hilar, and subcarinal lymph nodes. This case represents an atypical imaging manifestation of organizing pneumonia that may lead to biopsy for a histopathologic diagnosis. After 14 months, the consolidation had resolved at imaging (not shown), despite continued ibrutinib therapy and without steroid treatment.

(18,19). FDG PET/CT features of radiation-induced acute pneumonitis include markedly FDG-avid consolidation and GGO within the irradiated field (Fig 5B); however, rarely, involvement outside of the radiation port is seen (18,20). If the acute postradiation pneumonitis is mild, then it may resolve with restoration of the normal lung parenchyma. However, if the postradiation pneumonitis is severe, the acute exudative phase will progress to a proliferative phase at 3–9 months following XRT completion, with evolution to late pneumonitis or fibrosis at 9 months to 2 years (18,20).

At imaging, the proliferative phase is characterized by more focal organized consolidation, with decreasing FDG uptake relative to the

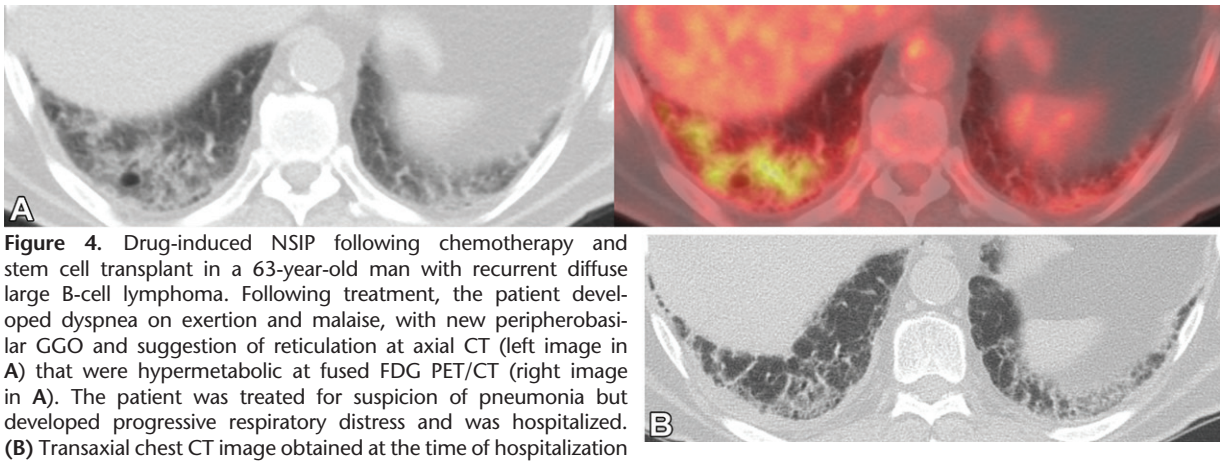

Figure 4. Drug-induced NSIP following chemotherapy and stem cell transplant in a 63-year-old man with recurrent diffuse large B-cell lymphoma. Following treatment, the patient developed dyspnea on exertion and malaise, with new peripherobasilar GGO and suggestion of reticulation at axial CT (left image in **A**) that were hypermetabolic at fused FDG PET/CT (right image in **A**). The patient was treated for suspicion of pneumonia but developed progressive respiratory distress and was hospitalized. **(B)** Transaxial chest CT image obtained at the time of hospitalization shows peripherobasilar reticulation with associated patchy GGO, most consistent with NSIP pattern pneumonitis that is probably secondary to gemcitabine and/or carmustine chemotherapy. Following steroid therapy for pneumonitis, the patient improved clinically, and follow-up FDG PET/CT (not shown) demonstrated decreased FDG uptake associated with bibasilar reticulation and patchy GGO.

uptake during the acute pneumonitis phase. The gradual transition from the proliferative phase to late pneumonitis or fibrosis is evident by progressive fibrotic changes, including volume loss, architectural distortion, and traction bronchiectasis with associated mild FDG avidity (Fig 5C). Following XRT for primary lung malignancy, the sensitivity of FDG PET/CT for detecting residual viable tumor is limited during the acute phase owing to diffuse hypermetabolic activity from acute pneumonitis within the radiation field. Given this, it is optimal to perform FDG PET/CT at least 3 months after XRT completion (21).

Signs of recurrent disease include focal FDG activity within the irradiated field in the late phase, a new convex contour or lobulation seen at CT, and new focal airway obstruction in the area of late pneumonitis changes (18,20). Radiation recall pneumonitis may be seen in the irradiated field following the initiation of chemotherapy, targeted therapy, or immunotherapy agents. This is a delayed adverse effect that may occur 6 months to years following the completion of XRT (22).

Immunosuppression and Invasive Fungal Pneumonia

Immunosuppression such as neutropenia from intensive chemotherapy or stem cell transplant predisposes oncologic patients to pneumonia from typical bacterial organisms, fungi, viruses, and mycobacteria, with various pathogens (23). A comprehensive radiologic review of the infections in immunosuppressed patients is beyond the scope of this article; thus, we provide a brief discussion limited to invasive fungal pneumonias in patients with neutropenia.

Overall, bacterial organisms are the most common cause of neutropenic pneumonia; however, invasive fungal pneumonia is of particular concern, given the significant morbidity and mortality associated with this infection. *Aspergillus* is the most common pathogen in the invasive fungal pneumonias in neutropenic patients. Typical CT features of angioinvasive fungal pneumonias include parenchymal nodules and consolidation, often with surrounding GGO resulting from associated hemorrhage, providing the characteristic halo sign. Associated cavitation and pulmonary infarcts also are often seen (24).

Various invasive fungal pneumonias may mimic malignancy, with hypermetabolic pulmonary nodules or masses seen at FDG PET/CT, hypermetabolic lymphadenopathy, and disseminated disease, including aspergillosis, cryptococcosis, and mucormycosis (Fig 6) (25–27). Although invasive fungal pneumonias are more commonly associated with treatment of hematologic malignancies and stem cell transplant, they may also occur following treatment of solid-organ malignancies and may mimic progression of lung cancer in particular (26). Because patients with invasive fungal pneumonias such as aspergillosis and mucormycosis often have clinical symptoms of a rapidly progressive respiratory illness, correlating the symptoms with the clinical history is key to avoiding mistaking the pneumonia for a primary lung malignancy or metastases (27). However, sometimes clinical symptoms that are suggestive of infection are not readily apparent. Given this, invasive fungal pneumonia is an important differential consideration for new hypermetabolic pulmonary nodules or masses that are concerning for metastasis or malignant recurrence, especially in patients with immunosuppression, which in many cases cannot be distinguished on the basis of clinical and radiologic findings and may require biopsy for a histopathologic diagnosis.

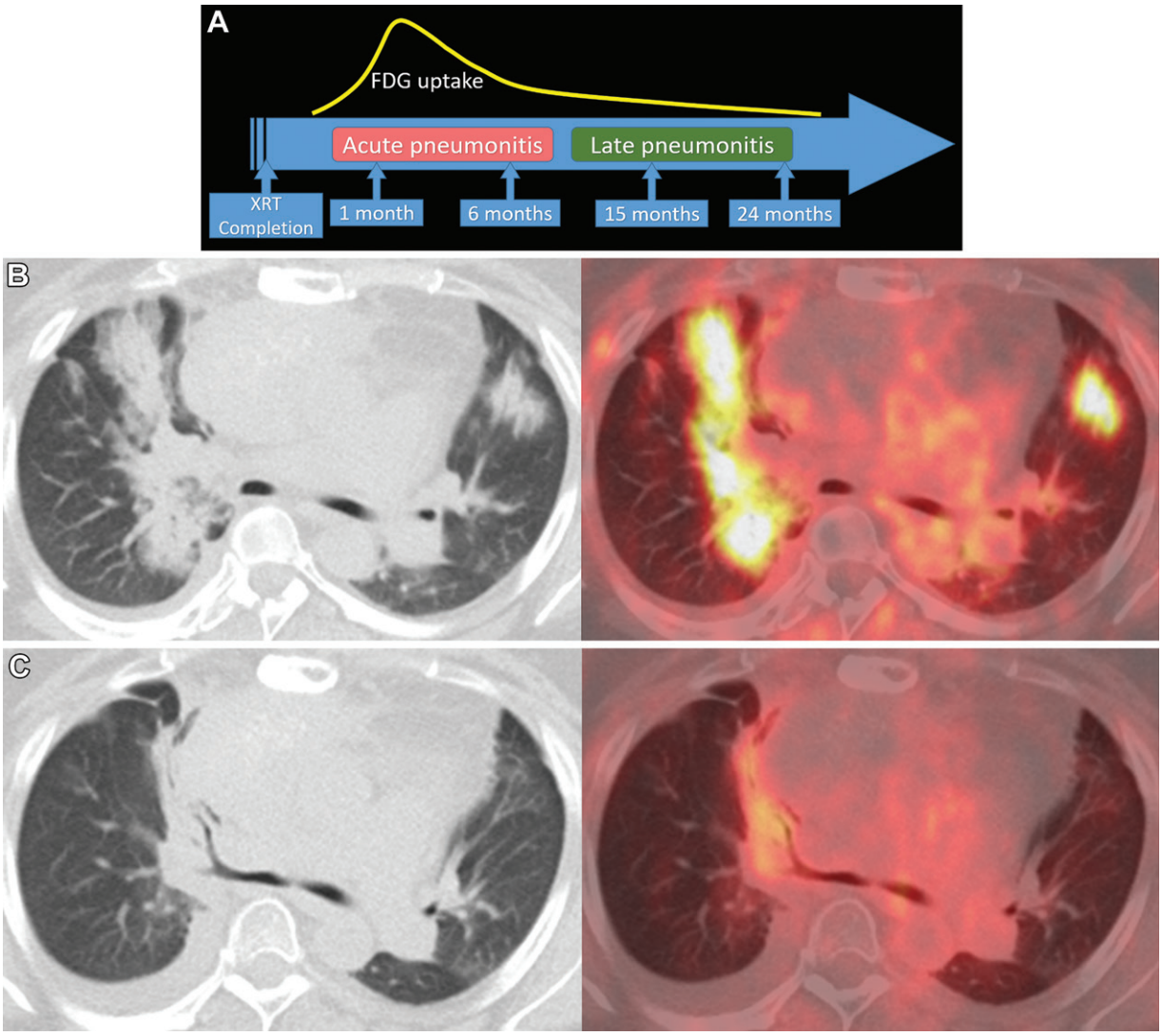

Figure 5. Radiation-induced pneumonitis in a 47-year-old woman. **(A)** Diagram depicting the time course of radiation-induced pneumonitis following completion of XRT demonstrates the trend of FDG uptake seen on FDG PET/CT images over time (18). **(B, C)** Transaxial CT (left) and fused FDG PET/CT (right) images show locally advanced squamous cell carcinoma of the thymus. **(B)** FDG PET/CT image (right) 3 months following completion of XRT shows new markedly hypermetabolic paramediastinal consolidation, greater on the right than on the left, consistent with acute radiation-induced pneumonitis. **(C)** Five months after XRT completion, there is evolution of right paramediastinal pneumonitis, with volume loss and decreased, mildly hypermetabolic activity; these findings are consistent with transition to late pneumonitis and scarring. The lingular hypermetabolic consolidation previously seen had resolved.

Additional less frequently encountered pulmonary parenchymal complications of oncologic therapy include pulmonary hemorrhage, specifically that related to the antiangiogenic agent bevacizumab (28). Pulmonary edema is another important pulmonary complication; it may be seen more commonly in patients with fluid overload.

Airway and Pleural Complications and Posttreatment Effects

Bronchopleural Fistula

Bronchopleural fistula (BPF) most commonly occurs as a postoperative complication following lung resection, although it is also an uncommon complication of necrotic lung masses, particularly after XRT and/or chemotherapy (29,30). Additional causes include chest trauma, necrotizing lung infections such as tuberculosis, and iatrogenic complications. On CT images, a direct communication between the airways or lung parenchyma and the pleural space may be evident, although a persistent hydropneumothorax or pneumothorax is an indirect sign that is highly suggestive. BPF is a relatively rare complication of oncologic treatment, and the acute presentation and initial diagnosis are much more likely to be identified with imaging modalities other than FDG PET/CT. However, several cases of chronic BPF developing after XRT or chronically persisting as a complication of prior surgery have been encountered at FDG PET/CT at our institution (Fig 7). CT features that are suggestive

Figure 6. Disseminated invasive fungal infection in an immunosuppressed oncologic patient, a 59-year-old man with Burkitt lymphoma of the transverse colon who was treated with chemotherapy. After receiving the final cycle of chemotherapy, the patient developed neutropenia complicated by fungal pneumonia (presumably angioinvasive aspergillosis). Whole-body maximum intensity projection PET image **(A),** and axial lung-window **(B)** and soft-tissue–window **(C)** fused FDG PET/CT images following completion of chemotherapy show multiple new hypermetabolic pulmonary nodules and necrotic masses (solid arrows in **A,** arrows in **B**), hilar and mediastinal lymphadenopathy (arrowheads in **A** and **B**), and a left thigh mass (dashed arrow in **A** and **C**), compatible with disseminated fungal infection. Biopsy of the left thigh mass yielded fungal elements without evidence of lymphoma. The patient improved clinically with antifungal therapy, with marked improvement of the imaging findings seen at follow-up FDG PET/CT.

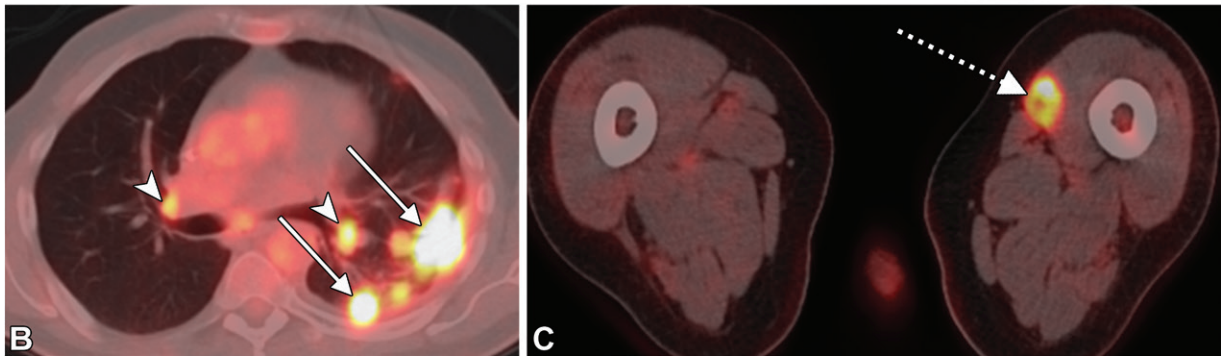

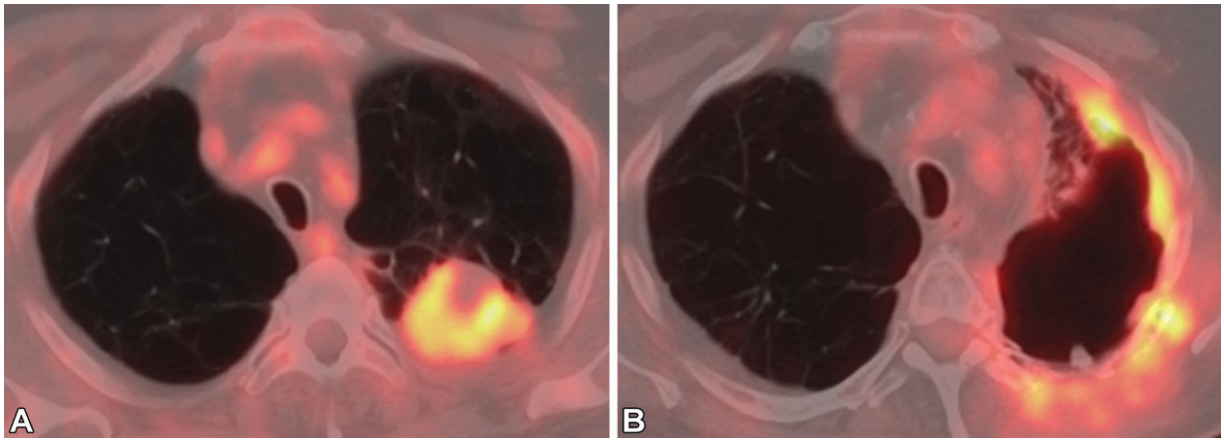

Figure 7. XRT-associated BPF in a 72-year-old man with left upper lobe non–small cell lung cancer. **(A)** Transaxial FDG PET/CT image before treatment shows a hypermetabolic mass corresponding to the patient's primary left upper lobe malignancy, with underlying extensive biapical predominant emphysematous changes. Following definitive XRT, CT surveillance imaging (not shown) showed progressive post-XRT changes, with development of a loculated left apical pneumothorax 18 months after XRT and a direct communication with the bronchial tree seen at diagnostic chest CT, consistent with a BPF. **(B)** Subsequent transaxial FDG PET/CT image 5 years after XRT shows the known left upper lobe BPF with mild to moderate hypermetabolic activity along the walls of the loculated pneumothorax with corresponding pleural thickening. Considering that the CT findings were stable compared to multiple prior imaging studies, the current appearance was favored to represent inflammatory uptake rather than recurrent malignancy. Continued CT surveillance (not shown) demonstrated stable findings without evidence of disease recurrence.

of chronic BPF include a loculated pneumothorax with surrounding pleural thickening, with either a directly visualized fistula to the airways or progressively increased size of the air-filled cavity indirectly indicating a fistula. Characteristic FDG PET/CT findings of XRT-induced BPF have not been reported, but expected and observed findings from our experience include FDG-avid pleural thickening with associated chronic loculated pneumothorax or hydropneumothorax.

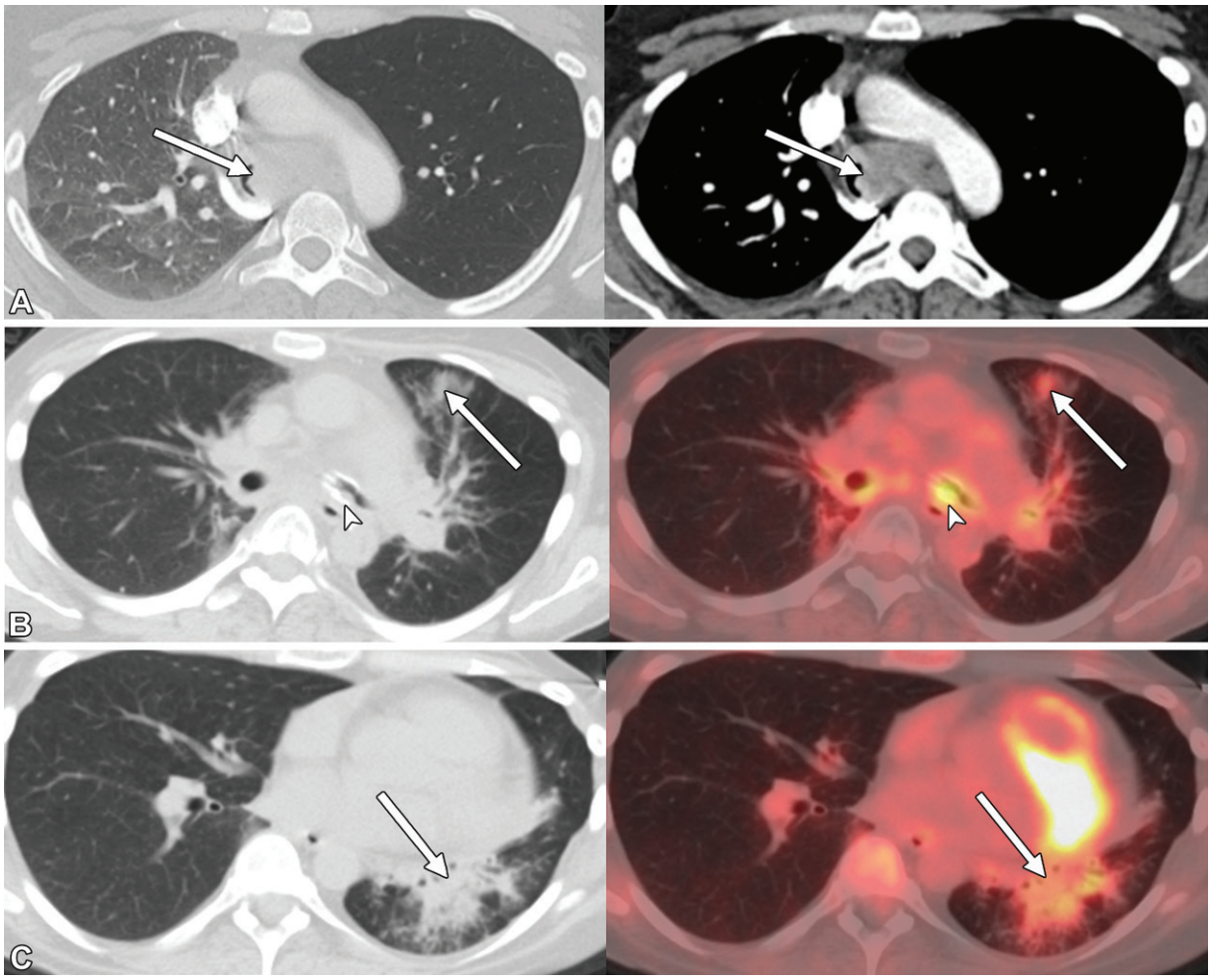

Figure 8. Chemoradiation therapy–associated bronchoesophageal fistula in a 57-year-old woman with adenoid cystic carcinoma of the trachea. **(A)** Initial transaxial lung-window (left) and soft-tissue–window (right) CT images show the primary tracheal mass (arrows), resulting in stenosis of the right main bronchus and complete occlusion of the left main bronchus with associated right lung atelectasis and left-lung air trapping, respectively. The patient was treated with stent placement in the trachea and left main bronchus followed by chemoradiation therapy. Posttreatment CT images during the next year showed recurrent aspiration with sequelae of chronic aspiration (not shown) that was concerning for esophageal-airway fistula. Esophagram findings confirmed a fistula near the level of the left main bronchus origin (Fig E1). **(B, C)** Subsequent restaging transaxial CT (left) and fused FDG PET/CT (right) images at the level of the mid thorax **(B)** and lower thorax **(C)** show changes of acute-on-chronic aspiration in the left lung with associated mildly hypermetabolic activity, including patchy tree-in-bud nodules and small nodular consolidation in the left lung (arrows in **B**) with consolidation and volume loss suggestive of scarring predominantly within the left lower lobe (arrows in **C**). The fistula was not directly visualized with CT. Hypermetabolic activity along the central airways, including the stented left main bronchus (arrowheads in **B**), most likely represents inflammatory changes related to treatment and aspiration, limiting evaluation for residual or recurrent disease.

Airway-Esophageal Fistula

Acquired tracheoesophageal and bronchoesophageal fistulas most commonly occur in patients with mediastinal malignancies, particularly esophageal cancer, before or after treatment with XRT and/or chemotherapy. Less common causes include endotracheal tube–related injury, postsurgical complications, trauma, ingestion of caustic substances, and rarely, granulomatous infection (31,32). Although a direct communication may be visualized with CT, the fistula tract may be collapsed at the time of imaging. Given this, if there is a clinical concern, fluoroscopic or CT esophagography should be performed to confirm the presence or absence of a fistula.

Indirect CT findings of airway-esophageal fistula include recurrent aspiration with dependent acute-on-chronic inflammatory changes, and this may be the initial sign that triggers further evaluation (31,32). Characteristic FDG PET/CT findings of treatment-related airway-esophageal fistula have not been reported. In a case of confirmed bronchoesophageal fistula involving the left main bronchus at our institution, CT findings were acute-on-chronic aspiration pneumonitis in the left lung with associated mild FDG avidity, as well as hypermetabolic activity along the central airways that was likely predominantly inflammatory, related to aspiration and treatment (Figs 8, E1).

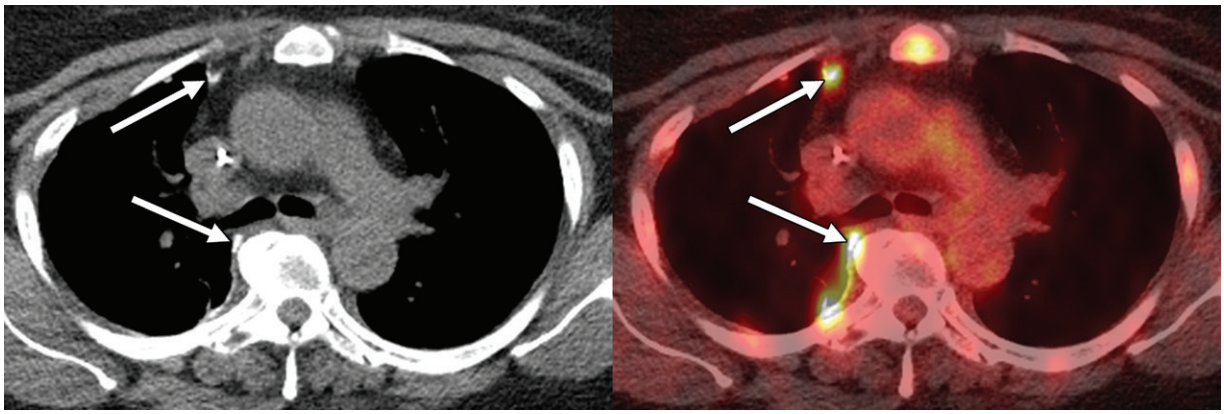

Figure 9. Findings after talc pleurodesis for recurrent right pleural effusion in a 59-year-old woman with acute lymphocytic leukemia. Restaging transaxial CT (left) and fused FDG PET/CT (right) images show focal right pleural FDG uptake (arrows in right image) with corresponding high-attenuation foci at CT (arrows in left image), compatible with inflammatory changes from talc pleurodesis performed 1 year ago. Focal uptake in the sternum is favored to represent leukemic involvement.

Talc Pleurodesis

Talc pleurodesis is a treatment for persistent pleural effusion or pneumothorax that may be encountered in oncologic patients and is notable for associated persistent inflammatory pleural FDG avidity in patients following treatment. While inflammatory pleural FDG avidity is not a complication, it is important to be aware of this expected posttreatment finding that may mimic malignancy. Pleural talc administration results in an inflammatory response that promotes pleurodesis, with histopathologic analysis demonstrating formation of pleural granulomata that evolves to pleural fibrosis (33,34). On FDG PET/CT images, there is increased pleural uptake, which may be linear or focal and may persist for more than 10 years following the procedure (34,35) (Fig 9). On CT images, there are corresponding areas of pleural thickening or nodularity with high-attenuation foci on noncontrast images corresponding to pleural talc (Fig 9), which is a helpful CT correlate that suggests this diagnosis, even if the clinical history is lacking.

Systemic Complications

Immune-related Adverse Events

A variety of irAEs have been associated with immune checkpoint inhibitors, and these can manifest in any organ (36,37). Active inflammation resulting from irAEs is often readily evident on FDG PET/CT images, and it is important to be aware of the imaging manifestations of this condition to provide a prompt diagnosis and distinguish it from recurrent malignancy (38). Pneumonitis is an important potentially life-threatening irAE, with a reported prevalence of 11.8% with nivolumab therapy. Most cases (65%) of this pneumonitis demonstrate a CT pattern of organizing pneumonia (Fig 1), although a wide spectrum of lung injury patterns have been observed. Additional lung injury patterns include NSIP, hypersensitivity pneumonitis pattern, and acute interstitial pneumonia, the latter of which is associated with the highest toxicity grade (36,39). Additional thoracic irAEs include SLG (discussed in the next section), bronchitis, pleuritis, myocarditis, pericarditis, and esophagitis (37).

Sarcoid-like Granulomatosis

SLG is an adverse event with thoracic manifestations that can mimic recurrent malignancy. It manifests with characteristic imaging and histologic findings of sarcoidosis that typically involve the lungs, as well as mediastinal and hilar lymph nodes, although it may involve other lymph node regions and the spleen, among other organs. In addition to being an irAE associated with various immune checkpoint inhibitors, SLG has long been reported to have a broader relationship with cancer, with an unclear pathologic mechanism (40).

While some retrospective studies have attributed SLG to an adverse effect of chemotherapies, investigators in multiple reports (40,41) have shown that many oncologic patients with SLG did not receive chemotherapy and have hypothesized that SLG may represent an immunologic response to malignancy. Retrospective studies have shown that the overall median interval between the diagnosis of cancer and the subsequent diagnosis of SLG is approximately 3 years (41). However, in patients treated with immune checkpoint inhibitor therapy, the reported median time from immunotherapy initiation to SLG diagnosis is 14 weeks (42). Characteristic FDG PET/CT features of SLG include FDG-avid pulmonary micronodules or focal round consolidation with surrounding GGO; symmetric FDG-avid lymphadenopathy, typically with mediastinal and hilar involvement; and hypermetabolic splenic lesions

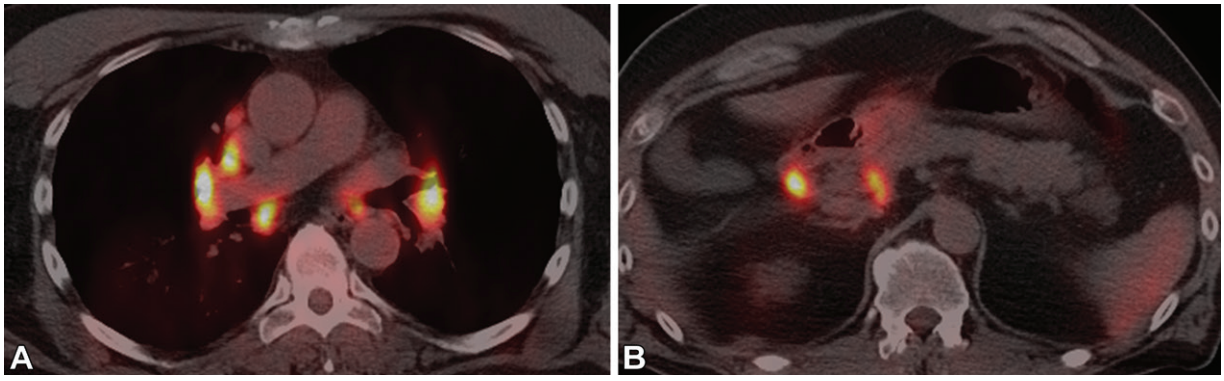

Figure 10. SLG with lymphadenopathy in a 67-year-old man with metastatic melanoma that was treated with checkpoint inhibitor immunotherapy (ipilimumab plus nivolumab). Transaxial FDG PET/CT images obtained at the levels of the mid thorax **(A)** and upper abdomen **(B)** to monitor treatment response show new hypermetabolic bilateral hilar, mediastinal, and periportal lymphadenopathy. Subsequent biopsy of bilateral hilar and right paratracheal lymph nodes showed granulomatous inflammation consistent with SLG.

(Fig 10) (38,42,43). Care should be taken not to mistake SLG for hyperprogression or pseudoprogression after immunotherapy.

Mediastinal Complications

Rebound Thymic Hyperplasia

Both physiologic thymic FDG uptake and post-chemotherapy thymic hyperplasia are common in patients younger than 20 years but less commonly seen in older adults (44,45). Thymic hyperplasia occurs owing to a rebound phenomenon of the immune system following an event that causes thymic aplasia; this has been described following chemotherapy in addition to a variety of acute stress events (46). Thymic hyperplasia typically occurs 3–14 months after the initiation of chemotherapy, but it may be delayed for up to 5 years. On FDG PET/CT images, the thymus is enlarged and often has diffuse marked FDG uptake (Fig 11). Features that distinguish thymic hyperplasia from malignant involvement include diffuse enlargement, smooth contour, maintained typical inverted Y configuration on coronal images, and normal intervening fat, lymphoid tissue, and vasculature.

In contrast, thymic malignancy is characterized by a focal mass or nodular contour with complex features such as areas of necrosis or calcification (46). If there is any radiologic uncertainty regarding thymic tissue versus a mediastinal mass, chest MRI can be helpful in characterizing thymic tissue, which characteristically loses signal with T1-weighted opposed-phase sequences. Alternatively, short-interval follow-up chest CT may be performed, with decreased thymic size at follow-up in the absence of further therapy being indicative of resolving thymic hyperplasia.

Esophagitis

Treatment-related esophagitis can develop secondary to chemotherapy, immunotherapy, or XRT. Risk factors for radiation-induced esophagitis include radiation dose and concurrent chemotherapy administration (47). FDG PET/CT demonstrates increased linear FDG uptake along the esophagus, with correlate CT findings of esophageal wall thickening. Radiation-induced esophagitis demonstrates sharply demarcated cranial and caudal margins of involvement corresponding to the radiation field (18). In primary esophageal malignancy, focal FDG uptake is concerning for recurrence. Complications of treatment-related esophagitis include ulcer, perforation, and typically later, fistula formation and stricture.

Cardiovascular Complications

Pericarditis

Multiple chemotherapies such as cyclosphosphamide and cytarabine, as well as checkpoint inhibitor immunotherapy agents, have been reported to be associated with acute pericarditis, although such cases are rare and mainly limited to case reports (37,48). XRT may cause acute or chronic pericardial disease if the pericardium is included in the radiation field, although the incidence of radiation-induced pericarditis is decreasing owing to improved XRT technologies (18). The normal pericardium is less than 2 mm in thickness at CT, and pericardial recesses often contain small amounts of fluid. Imaging features of acute pericarditis include pericardial effusion, smooth pericardial thickening, and enhancement after contrast material administration (49). Reports of FDG PET/CT findings of inflammatory pericarditis, including chemotherapy-induced pericarditis, show heterogeneous mild to moderately increased pericardial FDG uptake without focal intense uptake (Fig 12) (50,51).

In contrast, more intense pericardial FDG uptake is typically suggestive of infection or malignancy, and a focal FDG-avid soft-tissue mass

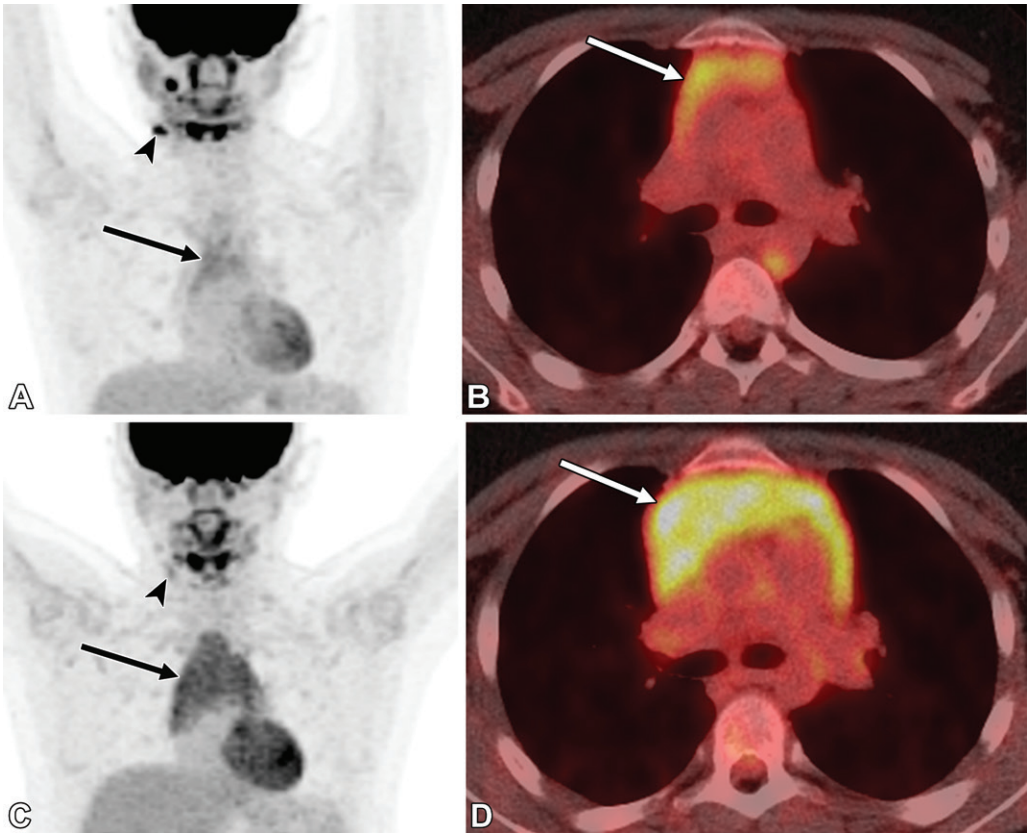

Figure 11. Rebound thymic hyperplasia in a 13-year-old boy with Hodgkin lymphoma following completion of chemotherapy. **(A, B)** Initial staging maximum intensity projection FDG PET **(A)** and transaxial fused FDG PET/CT **(B)** images show hypermetabolic right cervical lymphadenopathy consistent with biopsy-proven lymphoma (arrowhead in **A**), with physiologic thymic uptake seen in the anterior mediastinum (arrow). **(C, D)** Restaging maximum intensity projection PET **(C)** and transaxial fused FDG PET/CT **(D)** images 6 months after completion of chemotherapy show decreased avidity of the right cervical lymphadenopathy, consistent with treatment response (arrowhead in **C**). There is also interval diffusely increased size and activity of the thymus with maintained normal thymic morphology (arrow), most consistent with rebound thymic hyperplasia, which resolved at follow-up imaging without further treatment (not shown).

is highly suspicious for malignancy (52). Cardiac tamponade is a complication that may result from acute pericarditis with pericardial effusion. Imaging features of chronic pericarditis include pericardial thickening greater than 4 mm with or without pericardial calcifications and often predominantly over the right ventricle (RV)–anterior atrioventricular groove, and FDG uptake may be present or absent, depending on whether there is active inflammation. Chronic pericarditis may be complicated by constrictive pericarditis, including effusive-constrictive pericarditis, an uncommon variant caused by the combination of tense pericardial effusion and constriction by a chronically inflamed thickened visceral pericardium (49).

Cardiotoxicity

Various chemotherapy, targeted therapy, and immunotherapy agents may result in cardiotoxicity with a wide range of reversible or irreversible effects. Anthracyclines such as doxorubicin are commonly used agents that cause cardiotoxicity, with a characteristic dose-dependent reduction in left ventricular ejection fraction. Given this, patients undergo cardiotoxicity surveillance imaging to detect a subclinical decline in left ventricular ejection fraction. These imaging examinations include multigated cardiac blood pool scanning, echocardiography, and MRI and enable early detection and therapy modification (53). Evaluation for cardiotoxicity with routine oncologic FDG PET/CT is largely limited owing to substantial variability in normal myocardial FDG uptake, which may be absent, diffusely increased, heterogeneously increased, focally increased (eg, papillary muscle uptake), or regionally increased (commonly with posterolateral activity greater than anteroseptal activity) (54). For dedicated cardiac FDG PET/CT, patient preparation with prolonged fasting and a low-carbohydrate diet can be used to suppress myocardial FDG uptake by shifting the myocardial metabolism to fatty acids and suppressing myocardial glycolysis (55). This substantially limits the variation in myocardial FDG uptake, and with appropriate patient preparation, cardiac FDG PET/CT has proven

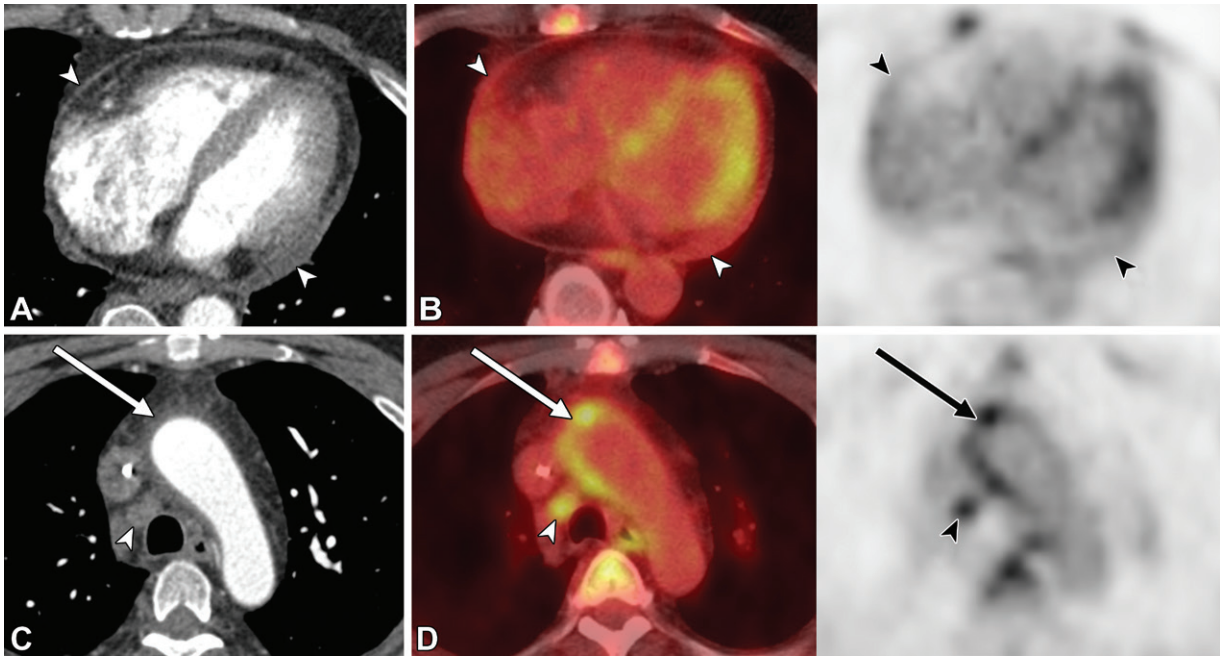

Figure 12. Chemotherapy-associated acute pericarditis in a 63-year-old woman with small cell carcinoma of the lung. After completion of cycle 3 of carboplatin-etoposide chemotherapy, the patient developed fevers and pleuritic chest pain. **(A, C)** Transaxial contrast-enhanced CT images show new mild pericardial thickening with trace pericardial fluid and mild adjacent fat stranding (arrowheads in **A**), including involvement of the superior aortic recess (arrow in **C**). **(B, D)** Transaxial fused FDG PET/CT (left) and PET (right) images show corresponding increased mild linear uptake along the right atrium and base of the left ventricle (arrowheads in **B**), as well as more avid uptake along the superior aortic recess (arrows in **D**), raising suspicion for acute pericarditis. The extent of increased activity along the ascending aorta is limited to the area of the superior aortic recess without circumferential aortic involvement, favoring acute pericarditis rather than aortitis. Although more focal uptake is seen in the superior aortic recess, no soft-tissue nodularity is seen at dedicated CT of the chest to suggest metastasis, and these findings had resolved at short-interval follow-up. Arrowheads in **C** and **D** denote an adjacent hypermetabolic right paratracheal nodal metastasis.

utility in the evaluation of inflammatory myocarditis such as cardiac sarcoidosis (55). In addition, list mode–driven gated acquisition can be used to limit motion artifact and improve cardiac PET.

Although cardiac evaluation with routine oncologic FDG PET/CT is limited owing to variable myocardial uptake, several retrospective studies have reported increased myocardial uptake in patients following anthracycline chemotherapy. One study (56) showed an association with decreased left ventricular ejection fraction, and another study (57) showed an association with cardiotoxicity. However, the potential role of FDG PET/CT in the evaluation of treatment-related cardiotoxicity remains unclear. In practice, fluctuation in myocardial FDG uptake in a given patient at serial routine oncologic FDG PET/CT is a nonspecific finding, and further research, including FDG PET/CT performed with dedicated cardiac protocol preparation, may be needed.

XRT can result in cardiotoxicity, depending on the radiation dose and the amount of the heart within the radiation field. Adverse effects include myocarditis, cardiomyopathy, valvular disease, and accelerated atherosclerosis. Radiation-induced cardiotoxicity often manifests clinically years after the completion of XRT, with an estimated prevalence of XRT-induced cardiac disease of 10%–30% (18,53). Multiple studies (58,59) have demonstrated focally increased myocardial FDG activity corresponding to the irradiated field, suggesting acute myocardial inflammation or damage. Increased myocardial activity associated with the irradiated field was not observed at early evaluation at 1 month, but it was present on FDG PET/CT images after several months and persisted beyond 1 year (58,59). Whether these observed areas of focally increased myocardial FDG activity are directly related to subsequent adverse cardiotoxic sequelae remains unclear. However, being aware that XRT may result in focal myocardial FDG uptake is important, to at least avoid mistaking this finding for metastatic disease, as demonstrated in one case report (60).

Vasculitis

Vasculitis is a rare but reported adverse effect of various chemotherapy agents such as gemcitabine, and targeted therapy and immunotherapy agents such as lenalidomide and immune checkpoint inhibitors (37,61). XRT can also cause vasculitis characterized by involvement within the radiation port (18). General CT and

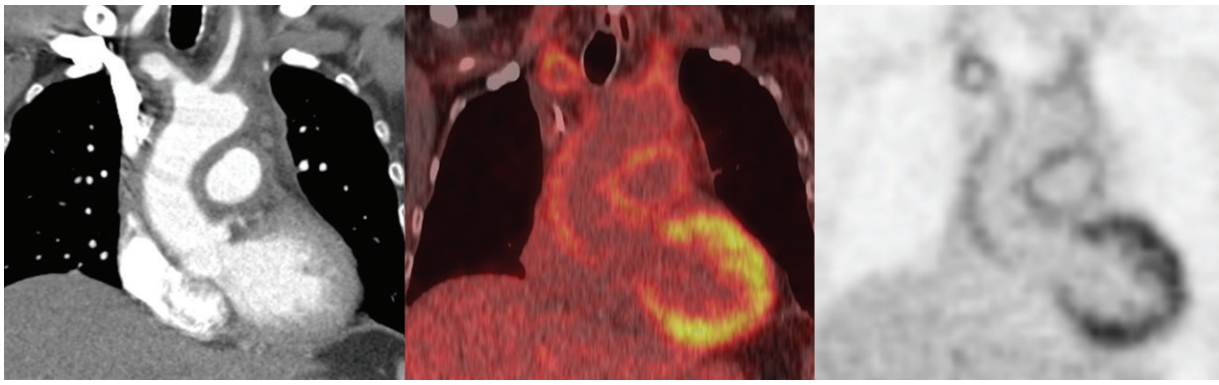

Figure 13. Lenalidomide-associated large-vessel vasculitis in a 47-year-old man with multiple myeloma. The patient presented with progressive subacute chest pain, shortness of breath, and fever. Evaluation with contrast-enhanced coronal CT (left image), fused FDG PET/CT (middle image), and PET (right image) was performed. Contrast-enhanced CT and FDG PET/CT images show new diffuse wall thickening of the aorta, great vessels, and pulmonary artery, with circumferential hypermetabolic activity. Infectious and rheumatologic workup results were negative, and the patient's symptoms and imaging findings resolved following steroid treatment and discontinuation of the current multiple myeloma therapy regimen, with transition to an alternative treatment regimen.

MRI findings of large- or medium-sized–vessel vasculitis include vessel wall thickening and enhancement with or without an abnormal vessel caliber such as narrowing, dilatation, or a beaded appearance (62). Small-vessel vasculitis involves vessels that are not resolved at CT or MRI; instead, it manifests indirectly as hemorrhage and/or end-organ failure due to inflammation and/or ischemia (62). Following XRT, long-segment, smooth, vascular stenosis of large vessels with vascular wall thickening confined to the region of the radiation port is characteristic of post-XRT vasculitis (18). Complications of vasculitis include occlusion and pseudoaneurysm. During active disease, FDG PET/CT demonstrates circumferentially increased activity within the thickened vessel walls, with a reported sensitivity of 77%–92% and reported specificity of 89%–100% for large-vessel vasculitis (Fig 13) (52).

Pulmonary Embolism

Venous thromboembolism is a significant source of morbidity and mortality in oncologic patients. The increased risk of venous thromboembolic disease in oncologic patients often involves multiple factors, including the patient's underlying malignancy itself, as well as various chemotherapy, targeted therapy, and immunotherapy agents (63). Oncologic FDG PET/CT examinations are commonly performed without intravenous contrast material, and recognition of the noncontrast CT findings of pulmonary embolism (PE) is important, as PE is often incidentally detected with surveillance imaging. Noncontrast CT findings of PE include direct and indirect findings, which have been assessed in studies involving patients with clinically suspected PEs. Hyperattenuating lumen, a direct sign, had a reported specificity of 99%–100% for central PE, with a high positive predictive value (89%–100%) (64–66). However, it has limited sensitivity and negative predictive value and is less specific for peripheral emboli (Fig 14A, 14B, 14D). A peripheral wedge-shaped opacity indicative of pulmonary infarction was found to be the most common indirect sign of PE at noncontrast CT in one study (Fig 15) (66).

Increased RV FDG uptake may be an indicator of RV strain, given that an increased RV–left ventricle FDG uptake ratio has been shown to correlate with increased pulmonary vascular resistance in patients with pulmonary arterial hypertension (67). In addition, increased RV FDG uptake was observed in a case of central PE at our institution, with follow-up contrast-enhanced CT showing evidence of RV strain (Fig 14C, 14E). In the cited studies of the noncontrast CT findings of PE, patients with clinically suspected PE were evaluated and sample sizes were relatively limited. Also, the utility of these noncontrast CT findings in guiding further evaluation for incidental PE remains to be determined. However, given the potential morbidity and mortality associated with missing PE, the application of these signs to suggest further imaging evaluation is reasonable in the high-risk oncologic patient population until more data are available.

Tumor thrombus may be seen with a variety of malignancies, commonly hepatocellular carcinoma and renal cell carcinoma. It is notable that both bland thrombus and tumor thrombus can demonstrate FDG avidity, although multiple retrospective studies have shown that higher uptake is indicative of tumor thrombus (Fig 16) (25). The FDG avidity of tumor thrombus correlates with that of the underlying malignancy, and focal uptake is suggestive of tumor thrombus, whereas linear intraluminal uptake is seen equally with bland thrombus and tumor thrombus. Contrast-

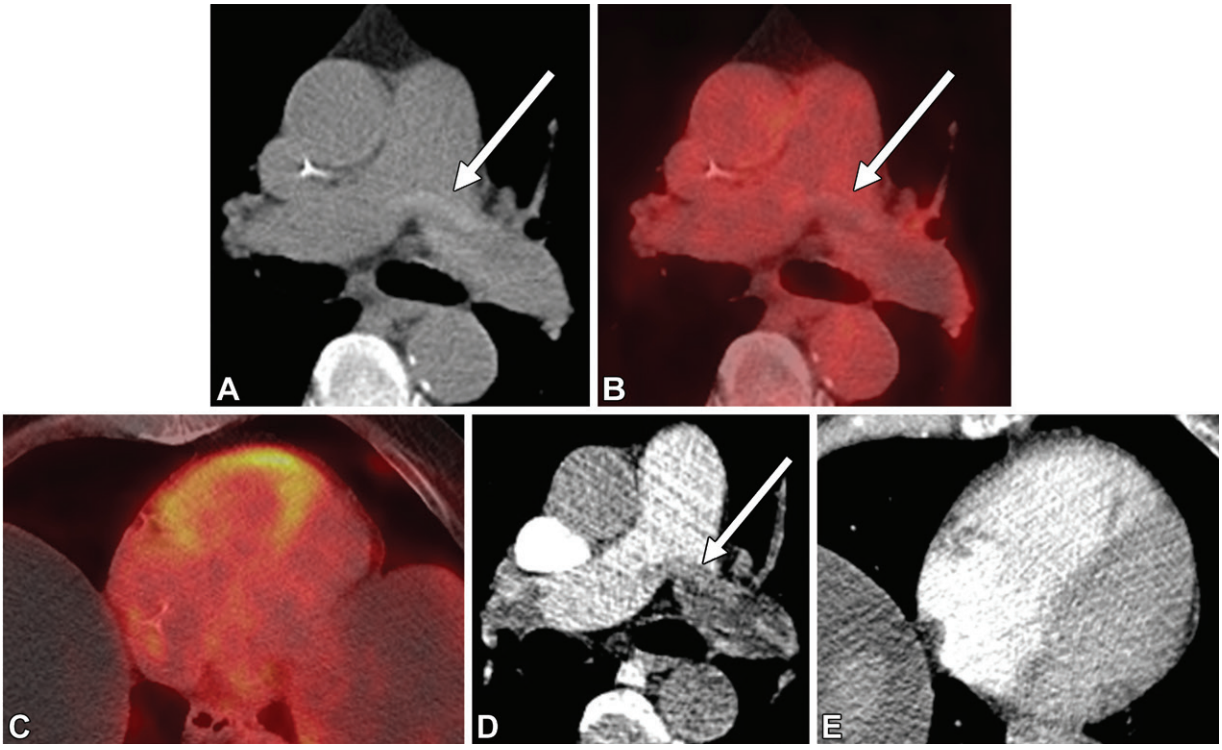

Figure 14. Hyperattenuating lumen sign, indicative of PE, in a 72-year-old man who presented for FDG PET/CT evaluation owing to suspected recurrence of pancreatic cancer. **(A, B)** Transaxial noncontrast CT **(A)** and fused FDG PET/CT **(B)** images show an incidentally noted hyperattenuating lumen sign (arrow) at the pulmonary artery bifurcation and left pulmonary artery without FDG avidity. **(C)** Transaxial fused FDG PET/CT image shows increased RV uptake, suggestive of RV strain. **(D, E)** Findings on subsequent contrast-enhanced transaxial CT images confirm the presence of central PE (arrow in **D**), with RV dilatation and a flattened interventricular septum, suggestive of RV strain (**E**).

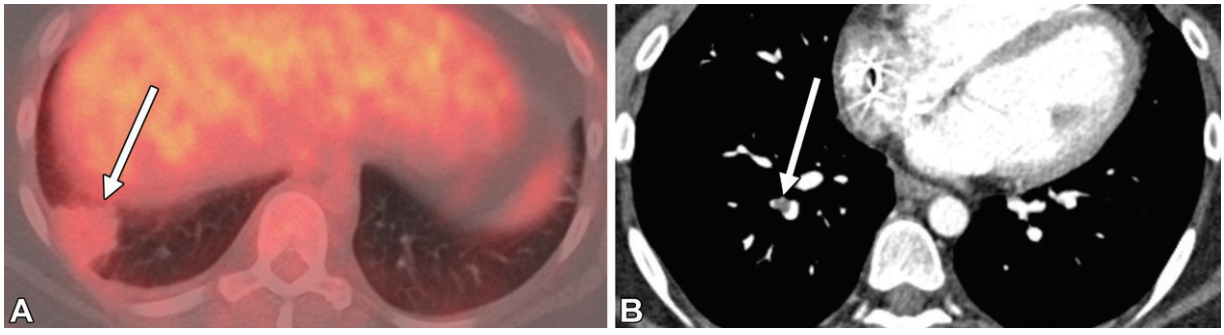

Figure 15. Peripheral consolidation concerning for possible pulmonary infarction in a 29-year-old woman with lymphoma who presented for restaging FDG PET/CT following recent completion of chemotherapy. **(A)** Transaxial fused FDG PET/CT image shows a peripheral wedge-shaped consolidation (arrow) with mild FDG avidity in the right lower lobe. The differential diagnosis included pulmonary infarction, resolving pneumonia, and less likely, tumor. **(B)** Subsequent contrast-enhanced CT image findings confirmed the presence of PE (arrow) in a segmental right lower lobe pulmonary artery.

enhanced CT findings also are helpful in differentiating tumor thrombus from bland thrombus, with the CT features suggestive of tumor thrombus including direct extension from extravascular tumor, intrathrombus enhancement, and marked venous expansion.

Skeletal and Soft-Tissue Complications

Radiation Osteitis and Osteoradionecrosis

Radiation osteitis develops within the irradiated field after a latent period owing to damage of osteoblasts and resultant bone matrix resorption. XRT initially results in osteopenia after approximately 1 year; subsequently, after 2–3 years, coarse trabeculae develop, with areas of mottled osteopenia and sclerosis. The late findings of radiation osteitis have been described as having features similar to Paget disease but without bone expansion (68). Rarely, radiation osteitis progresses to osteoradionecrosis, particularly following high XRT doses, and patients may have pain and increased metabolic activity on FDG PET/CT images years later, mimicking recurrent

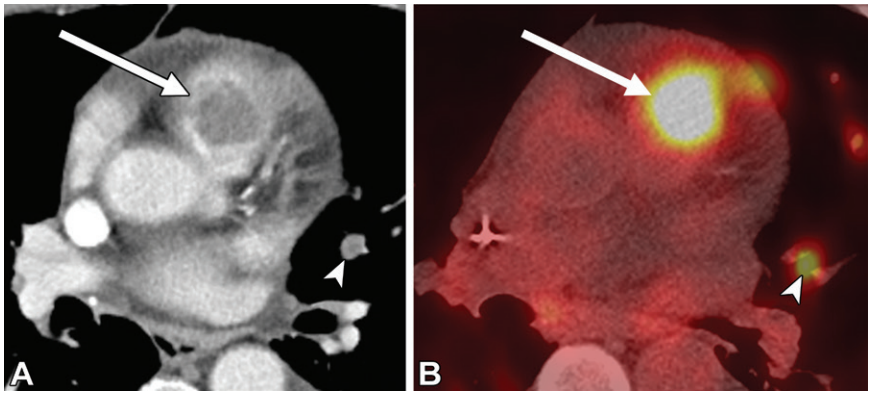

Figure 16. Metastatic renal cell carcinoma complicated by tumor thrombus in an 82-year-old man. Transaxial contrast-enhanced CT **(A)** and FDG PET/CT **(B)** images show a mass (arrow), which is markedly FDG-avid in **B,** within the right ventricular outflow tract extending into the main pulmonary artery, consistent with tumor thrombus, which was subsequently surgically excised. Hypermetabolic pulmonary nodules (arrowhead) also are seen.

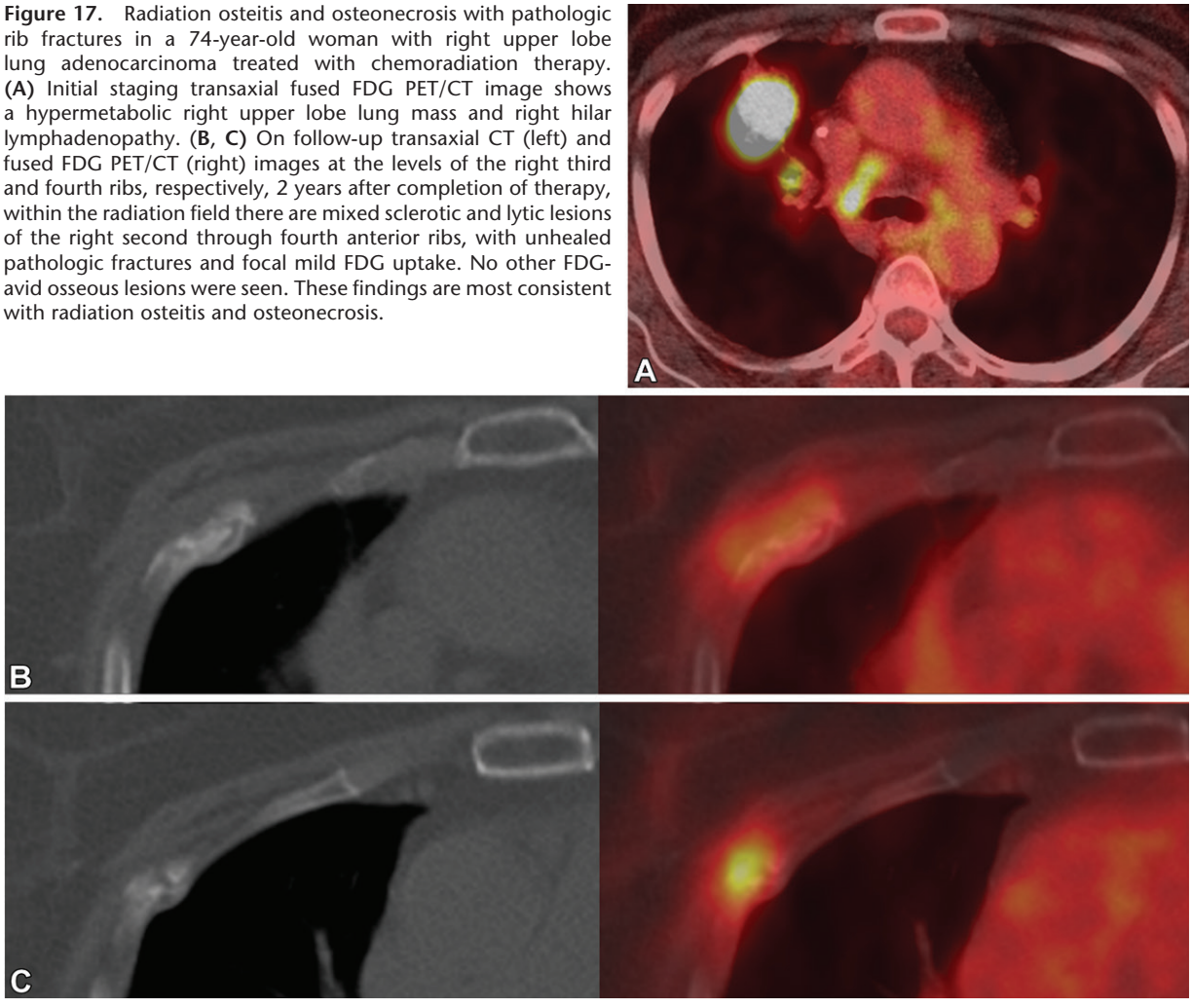

Figure 17. Radiation osteitis and osteonecrosis with pathologic rib fractures in a 74-year-old woman with right upper lobe lung adenocarcinoma treated with chemoradiation therapy. **(A)** Initial staging transaxial fused FDG PET/CT image shows a hypermetabolic right upper lobe lung mass and right hilar lymphadenopathy. **(B, C)** On follow-up transaxial CT (left) and fused FDG PET/CT (right) images at the levels of the right third and fourth ribs, respectively, 2 years after completion of therapy, within the radiation field there are mixed sclerotic and lytic lesions of the right second through fourth anterior ribs, with unhealed pathologic fractures and focal mild FDG uptake. No other FDG-avid osseous lesions were seen. These findings are most consistent with radiation osteitis and osteonecrosis.

or metastatic malignancy (Fig 17) (69). Radiation osteitis and osteoradionecrosis also predispose individuals to pathologic fractures (Figs 17, 18). CT findings of osteoradionecrosis, including lack of a soft-tissue mass and characteristic sclerosis, can help distinguish this condition from recurrent malignancy (68,69). Risk factors for radiation-induced osteoradionecrosis include high radiation dose, high radiation beam energy, and osteoporosis (68).

Radiation-induced Sarcomas

Radiation-induced sarcomas, although a rare complication of XRT, are of growing concern, given the increased long-term survival of oncologic patients with the current improved oncologic therapies. The incidence of sarcoma varies according to the radiation dose, irradiated organs and tissue, patient age, and hereditary factors (70). One study (71) reported the cumulative prevalence of radiation-induced sarcoma in

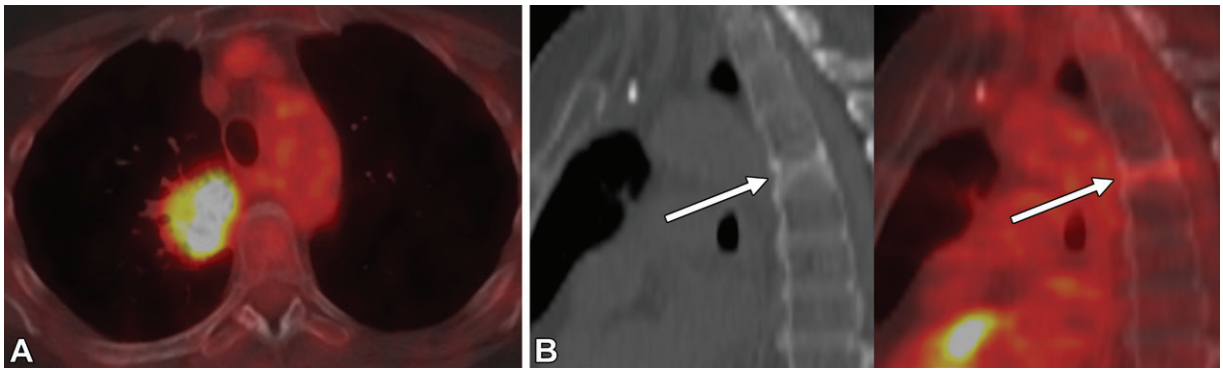

Figure 18. Radiation osteitis with pathologic vertebral compression fracture in a 67-year-old woman with right upper lobe squamous cell carcinoma following chemoradiation therapy. **(A)** Initial staging fused FDG PET/CT image shows a markedly hypermetabolic mass abutting the pleura adjacent to the T5 vertebral body. **(B)** At restaging FDG PET/CT performed 9 months after chemoradiation therapy, the right upper lobe lung mass is decreased in size, consistent with treatment response (not shown), although sagittal CT (left) and fused FDG-PET/CT (right) images show that a new T5 compression fracture (arrows) with mildly increased metabolic activity has developed. In addition, decreased uptake in the marrow in the upper to mid thoracic spine is seen at levels above and below the T5 vertebral level within the irradiated field. These findings are most consistent with a subacute to chronic pathologic compression fracture secondary to radiation osteitis, and subsequent surveillance imaging findings confirmed the absence of recurrent disease (not shown).

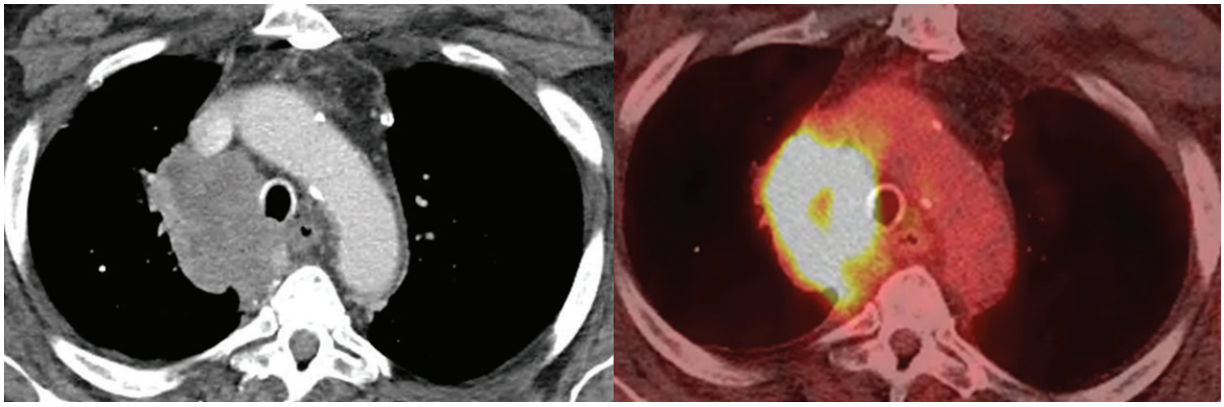

Figure 19. Radiation-induced sarcoma in a 63-year-old man with a remote history of Hodgkin lymphoma, treated with chemoradiation therapy, approximately 30 years earlier. Transaxial CT (left) and fused FDG PET/CT (right) images show a large markedly hypermetabolic right suprahilar-paratracheal mass with areas of necrosis. Histopathologic analysis confirmed radiation-associated sarcoma.

patients with breast cancer to be 0.48% at 15 years. Diagnostic criteria for radiation-induced sarcomas include tumor arising within a prior radiation field after a latent period of several years (typically 5–20 years) following completion of XRT, and confirmation of sarcoma that is distinct from the primary tumor at histopathologic analysis (70). Radiation-induced sarcomas are most commonly soft-tissue sarcomas, but osteosarcomas may be seen rarely. Radiation-induced sarcomas are typically poorly differentiated and high grade with markedly hypermetabolic activity at FDG PET/CT (70) (Fig 19). Poor prognostic indicators include central tumor location, incomplete surgical resection, microscopic tumor necrosis, and metastatic disease at diagnosis (72).

Other Soft-Tissue Complications

Additional soft-tissue complications of XRT include myositis, osteopenia, skin thickening, and fat necrosis. Gynecomastia can be seen as a result of targeted therapies, specifically in patients with prostate cancer who are receiving androgen deprivation therapy and in association with the tyrosine kinase inhibitor sunitinib (73,74). The differential diagnosis for gynecomastia is broad and includes chronic medical conditions such as cirrhosis and hypogonadism, conditions related to the use of various medications and supplements, and rarely, neoplasms such as prolactinomas.

Conclusion

FDG PET/CT has an important role in directing therapy for oncologic patients. Although this examination is routinely performed to detect malignancy and assess tumor treatment response, a critical role in interpreting FDG PET/CT image findings is to recognize adverse effects of therapy that may not be clinically suspected. A broad scope of treatment-related adverse effects with imaging manifestations are encountered. The diversity of treatments and associated complications

requires careful consideration of imaging findings within the context of the patient's therapeutic history. A cognizant radiologist's early detection of adverse effects is key in alerting the treating physician to guide prompt clinical management and further workup as needed.

***Disclosures of Conflicts of Interest*.—S.B.** *Activities related to the present article:* member of RSNA Board of Directors (not involved in the handling of this article). *Activities not related to the present article:* disclosed no relevant relationships. *Other activities:* disclosed no relevant relationships.

References

1. Carter BW, Erasmus JJ. Acute thoracic findings in oncologic patients. J Thorac Imaging 2015;30(4):233–246.
2. Meadors M, Floyd J, Perry MC. Pulmonary toxicity of chemotherapy. Semin Oncol 2006;33(1):98–105.
3. Vahid B, Marik PE. Pulmonary complications of novel antineoplastic agents for solid tumors. Chest 2008;133(2):528–538.
4. Nishino M, Hatabu H, Sholl LM, Ramaiya NH. Thoracic complications of precision cancer therapies: a practical guide for radiologists in the new era of cancer care. RadioGraphics 2017;37(5):1371–1387.
5. Rossi SE, Erasmus JJ, McAdams HP, Sporn TA, Goodman PC. Pulmonary drug toxicity: radiologic and pathologic manifestations. RadioGraphics 2000;20(5):1245–1259.
6. Kim SJ, Lee KS, Ryu YH, et al. Reversed halo sign on high-resolution CT of cryptogenic organizing pneumonia: diagnostic implications. AJR Am J Roentgenol 2003;180(5):1251–1254.
7. Ujita M, Renzoni EA, Veeraraghavan S, Wells AU, Hansell DM. Organizing pneumonia: perilobular pattern at thin-section CT. Radiology 2004;232(3):757–761.
8. Kligerman S, Raptis C, Larsen B, et al. Radiologic, pathologic, clinical, and physiologic findings of electronic cigarette or vaping product use-associated lung injury (EVALI): evolving knowledge and remaining questions. Radiology 2020;294(3):491–505.
9. Erdoğan Y, Özyürek BA, Özmen Ö, et al. The Evaluation of FDG PET/CT scan findings in patients with organizing pneumonia mimicking lung cancer. Mol Imaging Radionucl Ther 2015;24(2):60–65.
10. Tateishi U, Hasegawa T, Seki K, Terauchi T, Moriyama N, Arai Y. Disease activity and 18F-FDG uptake in organising pneumonia: semi-quantitative evaluation using computed tomography and positron emission tomography. Eur J Nucl Med Mol Imaging 2006;33(8):906–912.
11. Lee ST, Scott AM. Are we ready for dual-time point FDG PET imaging? J Med Imaging Radiat Oncol 2011;55(4):351–352.
12. Jamar F, Buscombe J, Chiti A, et al. EANM/SNMMI guideline for 18F-FDG use in inflammation and infection. J Nucl Med 2013;54(4):647–658.
13. Cordier JF. Organising pneumonia. Thorax 2000;55(4):318–328.
14. Poletti V, Romagnoli M, Piciucchi S, Chilosi M. Current status of idiopathic nonspecific interstitial pneumonia. Semin Respir Crit Care Med 2012;33(5):440–449.
15. Kligerman SJ, Groshong S, Brown KK, Lynch DA. Nonspecific interstitial pneumonia: radiologic, clinical, and pathologic considerations. RadioGraphics 2009;29(1):73–87.
16. Jacquelin V, Mekinian A, Brillet PY, et al. FDG-PET/CT in the prediction of pulmonary function improvement in nonspecific interstitial pneumonia: a pilot study. Eur J Radiol 2016;85(12):2200–2205.
17. Umeda Y, Demura Y, Ishizaki T, et al. Dual-time-point 18F-FDG PET imaging for diagnosis of disease type and disease activity in patients with idiopathic interstitial pneumonia. Eur J Nucl Med Mol Imaging 2009;36(7):1121–1130.
18. Benveniste MF, Gomez D, Carter BW, et al. Recognizing radiation therapy-related complications in the chest. RadioGraphics 2019;39(2):344–366.
19. Hanania AN, Mainwaring W, Ghebre YT, Hanania NA, Ludwig M. Radiation-induced lung injury: assessment and management. Chest 2019;156(1):150–162.
20. Choi YW, Munden RF, Erasmus JJ, et al. Effects of radiation therapy on the lung: radiologic appearances and differential diagnosis. RadioGraphics 2004;24(4):985–997; discussion 998.
21. Boellaard R, Delgado-Bolton R, Oyen WJG, et al. FDG PET/CT: EANM procedure guidelines for tumour imaging: version 2.0. Eur J Nucl Med Mol Imaging 2015;42(2):328–354.
22. Cousin F, Desir C, Ben Mustapha S, Mievis C, Coucke P, Hustinx R. Incidence, risk factors, and CT characteristics of radiation recall pneumonitis induced by immune checkpoint inhibitor in lung cancer. Radiother Oncol 2021;157:47–55.
23. Evans SE, Ost DE. Pneumonia in the neutropenic cancer patient. Curr Opin Pulm Med 2015;21(3):260–271.
24. Orlowski HLP, McWilliams S, Mellnick VM, et al. Imaging spectrum of invasive fungal and fungal-like infections. RadioGraphics 2017;37(4):1119–1134.
25. Sharma P, Mukherjee A, Karunanithi S, Bal C, Kumar R. Potential role of 18F-FDG PET/CT in patients with fungal infections. AJR Am J Roentgenol 2014;203(1):180–189.
26. Park M, Ho DY, Wakelee HA, Neal JW. Opportunistic invasive fungal infections mimicking progression of non-small-cell lung cancer. Clin Lung Cancer 2021;22(2):e193–e200.
27. Guimarães MD, Marchiori E, Meirelles GS, et al. Fungal infection mimicking pulmonary malignancy: clinical and radiological characteristics. Lung 2013;191(6):655–662.
28. Ito M, Niho S, Nihei K, Yoh K, Ohmatsu H, Ohe Y. Risk factors associated with fatal pulmonary hemorrhage in locally advanced non-small cell lung cancer treated with chemoradiotherapy. BMC Cancer 2012;12(1):27.
29. Stern EJ, Sun H, Haramati LB. Peripheral bronchopleural fistulas: CT imaging features. AJR Am J Roentgenol 1996;167(1):117–120.
30. Lois M, Noppen M. Bronchopleural fistulas: an overview of the problem with special focus on endoscopic management. Chest 2005;128(6):3955–3965.
31. Shah CP, Yeolekar ME, Pardiwala FK. Acquired tracheo-oesophageal fistula. J Postgrad Med 1994;40(2):83–84.
32. Chaky DM, Escamilla C, Sheridan PH, Deboer D. Adult bronchoesophageal fistula diagnosed on computed tomography. Radiol Case Rep 2015;3(2):126.
33. Kennedy L, Sahn SA. Talc pleurodesis for the treatment of pneumothorax and pleural effusion. Chest 1994;106(4):1215–1222.
34. Murray JG, Erasmus JJ, Bahtiarian EA, Goodman PC. Talc pleurodesis simulating pleural metastases on 18F-fluorodeoxyglucose positron emission tomography. AJR Am J Roentgenol 1997;168(2):359–360.
35. Peek H, van der Bruggen W, Limonard G. Pleural FDG uptake more than a decade after talc pleurodesis. Case Rep Med 2009;2009:650864.
36. Kalisz KR, Ramaiya NH, Laukamp KR, Gupta A. Immune checkpoint inhibitor therapy–related pneumonitis: patterns and management. RadioGraphics 2019;39(7):1923–1937.
37. Jamal S, Hudson M, Fifi-Mah A, Ye C. Immune-related adverse events associated with cancer immunotherapy: a review for the practicing rheumatologist. J Rheumatol 2020;47(2):166–175.
38. Kwak JJ, Tirumani SH, Van den Abbeele AD, Koo PJ, Jacene HA. Cancer immunotherapy: imaging assessment of novel treatment response patterns and immune-related adverse events. RadioGraphics 2015;35(2):424–437.
39. Nishino M, Ramaiya NH, Awad MM, et al. PD-1 Inhibitor-related pneumonitis in advanced cancer patients: radiographic patterns and clinical course. Clin Cancer Res 2016;22(24):6051–6060.
40. Grados A, Ebbo M, Bernit E, et al. Sarcoidosis occurring after solid cancer: a nonfortuitous association: report of 12 cases and review of the literature. Medicine (Baltimore) 2015;94(28):e928.
41. Murthi M, Yoshioka K, Cho JH, et al. Presence of concurrent sarcoid-like granulomas indicates better survival in cancer patients: a retrospective cohort study. ERJ Open Res 2020;6(4):00061-2020.

42. Gkiozos I, Kopitopoulou A, Kalkanis A, Vamvakaris IN, Judson MA, Syrigos KN. Sarcoidosis-like reactions induced by checkpoint inhibitors. J Thorac Oncol 2018;13(8):1076–1082.
43. Nishino M, Sholl LM, Awad MM, Hatabu H, Armand P, Hodi FS. Sarcoid-like granulomatosis of the lung related to immune-checkpoint inhibitors: distinct clinical and imaging features of a unique immune-related adverse event. Cancer Immunol Res 2018;6(6):630–635.
44. Ferdinand B, Gupta P, Kramer EL. Spectrum of thymic uptake at 18F-FDG PET. RadioGraphics 2004;24(6):1611–1616.
45. Brink I, Reinhardt MJ, Hoegerle S, Altehoefer C, Moser E, Nitzsche EU. Increased metabolic activity in the thymus gland studied with 18F-FDG PET: age dependency and frequency after chemotherapy. J Nucl Med 2001;42(4):591–595.
46. Nasseri F, Eftekhari F. Clinical and radiologic review of the normal and abnormal thymus: pearls and pitfalls. RadioGraphics 2010;30(2):413–428.
47. Nieder C, Imingen KS, Mannsåker B, Yobuta R, Haukland E. Risk factors for esophagitis after hypofractionated palliative (chemo) radiotherapy for non-small cell lung cancer. Radiat Oncol 2020;15(1):91.
48. Plana JC, Galderisi M, Barac A, et al. Expert consensus for multimodality imaging evaluation of adult patients during and after cancer therapy: a report from the American Society of Echocardiography and the European Association of Cardiovascular Imaging. J Am Soc Echocardiogr 2014;27(9):911–939.
49. Wang ZJ, Reddy GP, Gotway MB, Yeh BM, Hetts SW, Higgins CB. CT and MR imaging of pericardial disease. RadioGraphics 2003;23(Spec Issue):S167–S180.
50. Losik SB, Studentsova Y, Margouleff D. Chemotherapy-induced pericarditis on F-18 FDG positron emission tomography scan. Clin Nucl Med 2003;28(11):913–915.
51. Strobel K, Schuler R, Genoni M. Visualization of pericarditis with fluoro-deoxy-glucose-positron emission tomography/computed tomography. Eur Heart J 2008;29(9):1212.
52. James OG, Christensen JD, Wong TZ, Borges-Neto S, Koweek LM. Utility of FDG PET/CT in inflammatory cardiovascular disease. RadioGraphics 2011;31(5):1271–1286.
53. Walker CM, Saldaña DA, Gladish GW, et al. Cardiac complications of oncologic therapy. RadioGraphics 2013;33(6):1801–1815.
54. Maurer AH, Burshteyn M, Adler LP, Steiner RM. How to differentiate benign versus malignant cardiac and paracardiac 18F FDG uptake at oncologic PET/CT. RadioGraphics 2011;31(5):1287–1305.
55. Skali H, Schulman AR, Dorbala S. 18F-FDG PET/CT for the assessment of myocardial sarcoidosis. Curr Cardiol Rep 2013;15(4):352.
56. Sarocchi M, Bauckneht M, Arboscello E, et al. An increase in myocardial 18-fluorodeoxyglucose uptake is associated with left ventricular ejection fraction decline in Hodgkin lymphoma patients treated with anthracycline. J Transl Med 2018;16(1):295.
57. Borde C, Kand P, Basu S. Enhanced myocardial fluorodeoxyglucose uptake following Adriamycin-based therapy: evidence of early chemotherapeutic cardiotoxicity? World J Radiol 2012;4(5):220–223.
58. Jingu K, Kaneta T, Nemoto K, et al. The utility of 18F-fluorodeoxyglucose positron emission tomography for early diagnosis of radiation-induced myocardial damage. Int J Radiat Oncol Biol Phys 2006;66(3):845–851.
59. Evans JD, Gomez DR, Chang JY, et al. Cardiac 18F-fluorodeoxyglucose uptake on positron emission tomography after thoracic stereotactic body radiation therapy. Radiother Oncol 2013;109(1):82–88.
60. Kröpil P, Budach W, Bölke E, et al. Pitfalls in radiation oncology. "Myocardial metastasis" in PET-CT after palliative radiation treatment of the left 5th rib. Strahlenther Onkol 2012;188(4):359–362.
61. Osafehinti D, Zivari K. Case of stroke from cerebral vasculitis following carfilzomib, lenalidomide, and dexamethasone therapy in a patient with relapsing multiple myeloma. Case Rep Hematol 2019;2019:5180424.
62. Broncano J, Vargas D, Bhalla S, Cummings KW, Raptis CA, Luna A. CT and MR imaging of cardiothoracic vasculitis. RadioGraphics 2018;38(4):997–1021.
63. Oppelt P, Betbadal A, Nayak L. Approach to chemotherapy-associated thrombosis. Vasc Med 2015;20(2):153–161.
64. Hassan HGEMA, Khater NH, Elia RZ. Added value of hyperdense lumen sign in prediction of acute central and peripheral pulmonary embolism on non-contrast CT chest. Egypt J Radiol Nucl Med 2021;52(1):84.
65. Tatco VR, Piedad HH. The validity of hyperdense lumen sign in non-contrast chest CT scans in the detection of pulmonary thromboembolism. Int J Cardiovasc Imaging 2011;27(3):433–440.
66. Mohamed N, Othman M, Hassan L, Yousef H. The accuracy of non-contrast chest computed tomographic Scan in the detection of pulmonary thromboembolism. J Curr Med Res Pract 2019;4(1):61–66.
67. Fang W, Zhao L, Xiong CM, et al. Comparison of 18F-FDG uptake by right ventricular myocardium in idiopathic pulmonary arterial hypertension and pulmonary arterial hypertension associated with congenital heart disease. Pulm Circ 2012;2(3):365–372.
68. Bluemke DA, Fishman EK, Scott WW Jr. Skeletal complications of radiation therapy. RadioGraphics 1994;14(1):111–121.
69. Alhilali L, Reynolds AR, Fakhran S. Osteoradionecrosis after radiation therapy for head and neck cancer: differentiation from recurrent disease with CT and PET/CT imaging. AJNR Am J Neuroradiol 2014;35(7):1405–1411.
70. O'Regan K, Hall M, Jagannathan J, et al. Imaging of radiation-associated sarcoma. AJR Am J Roentgenol 2011;197(1):W30–W36.
71. Kirova YM, Vilcoq JR, Asselain B, Sastre-Garau X, Fourquet A. Radiation-induced sarcomas after radiotherapy for breast carcinoma: a large-scale single-institution review. Cancer 2005;104(4):856–863.
72. Bjerkehagen B, Småstuen MC, Hall KS, Skjeldal S, Smeland S, Fosså SD. Why do patients with radiation-induced sarcomas have a poor sarcoma-related survival? Br J Cancer 2012;106(2):297–306.
73. Dobs A, Darkes MJ. Incidence and management of gynecomastia in men treated for prostate cancer. J Urol 2005;174(5):1737–1742.
74. Ballardini P, Margutti G, Aliberti C, Manfredini R. Onset of male gynaecomastia in a patient treated with sunitinib for metastatic renal cell carcinoma. Clin Drug Investig 2009;29(7):487–490.